

Technical University of Crete
School of Mineral Resources Engineering
Division of Minerals Exploitation
Management of Mining/ Metallurgical Wastes and Rehabilitation of Contaminated Soils

Master Thesis Title:

Properties of ground waste concrete inorganic polymers containing CuO and ZnO nanoparticles

Aikaterini I. Vavouraki

A Thesis submitted for the Master of Science Degree
for the Graduate Program in 'Geotechnology and the Environment'

Chania, February 2022

Τριμελής Συμβουλευτική Επιτροπή:

Κομνίτσας Κωνσταντίνος, Καθηγητής (Επιβλέπων) (ΜΗΧΟΠ)

Βενιέρη Δανάη, Αναπλ. Καθ. (ΧΗΜΗΠΕΡ)

Ξεκουκουλωτάκης Νικόλαος, Επικ. Καθηγητής (ΧΗΜΗΠΕΡ)

“Learning is the only thing the mind never exhausts, never fears, and never regrets.”

Leonardo da Vinci

“To study and not think is a waste. To think and not study is dangerous.”

Confucius

Table of Contents

Acknowledgements.....	6
Abstract.....	8
Περίληψη.....	9
Aim of the study.....	10
1. Introduction.....	11
1.1 Inorganic polymers.....	14
1.2 CuO and ZnO nanoparticles and inorganic polymers.....	18
2. Materials & methods.....	20
2.1 Synthesis of CuO and ZnO nanoparticles.....	20
2.2 Preparation of inorganic polymers.....	20
2.3 Structure analysis and characterization.....	20
2.4 Antibacterial activity.....	21
3. Results & Discussion.....	23
3.1 Characterization of nanoparticles.....	23
3.2 Characterization of inorganic polymers from Ground Waste Concrete with nanoparticles.....	24
3.2.1 Mechanical strength.....	24
3.2.2 XRD analysis.....	25
3.2.3 Raman analysis.....	26
3.2.4 SEM/ EDS analysis.....	27
3.2.5 Pores, water absorption, sorptivity.....	29
3.2.6 Hg-porosimetry analysis.....	30
3.2.7 Thermogravimetric (TG) analysis.....	31
3.2.8 Antibacterial activity.....	32
Conclusions.....	34
References.....	35

Acknowledgements

It is with great pleasure that I acknowledge certain people- colleagues and friends that with their assistance contributed to my succeeding into completing this task.

I am indebted to Prof. K. Komnitsas for giving me the opportunity to join his laboratory group, Research Unit of Technologies for Management of Mining/ Metallurgical wastes & Rehabilitation of Contaminated Soils, Division of Minerals Exploitation, School of Mineral Resources Engineering (MRED), Technical University of Crete (TUC) and be part of the INVALOR project (www.invalor.org); his advices and support throughout the course of this thesis were strongly helpful and insightful.

I am grateful to Iosifina Gounaki and Assoc. Prof. Danae Venieri (Laboratory of Environmental Microbiology, School of Chemical Engineering & Environmental Engineering, TUC) for research collaboration in the framework of my diploma work, their recommendations, scientific contribution and fruitful discussions.

I also acknowledge Asst. Prof. N. Xekoukoulotakis for accepting to be a member of my Master Thesis.

I herein acknowledge the collaboration with D.K. Kanellopoulou (Laboratory of Physical Metallurgy, Materials & Metallurgy, Ceramics & Composite Materials, Department of Chemical Engineering, University of Patras) and P.G.K. Koutsoukos (Laboratory of Inorganic & Analytical Chemistry ChemengUpatras and ICE-HT/ FORTH) on performing XRD and SEM/EDS analyses, respectively and also, for their co-operation and scientific contribution. Additionally, I would like to thank A.S.B. Beobide (ICE-HT/ FORTH), A.K. Kritikaki (MRED, TUC) and S. Sfakiotakis S. (MRED, TUC), for their collaboration and analyses of Raman, Hg-porosimetry and, TGA measurements, respectively.

I am really glad to have had the opportunity to work with Dr. Vasiliki Karmali, Dr. Athanasia Soultana and Dr. Katerina Valouma and becoming friends. Also, I am lucky to work with new colleagues and meet new friends that inspire me beyond the perspective of this thesis.

Last but not least, I would like to thank my brother, Asst. Prof. Vasileios Vavourakis for giving me considerable thoughts and ideas to consider, particularly to start this master; my parents, Zacharenia and Ioannis and my kids, Joanna and Stefanos for their support and, patience, SMILE and LOVE.

The financial support by the project “INVALOR: Research Infrastructure for Waste Valorization and Sustainable Management” (MIS 5002495) which is implemented under the Action “Reinforcement of the Research and Innovation Infrastructure”, funded by the Operational Programme “Competitiveness, Entrepreneurship and Innovation” (NSRF 2014–2020) and co-financed by Greece and the European Union (European Regional Development Fund) is gratefully acknowledged.

This study has already been published:

Vavouraki, A.I., Gounaki, I., Venieri, D., **2021.** Properties of Inorganic Polymers Based on Ground Waste Concrete Containing CuO and ZnO Nanoparticles. *Polymers* 13, 2871, doi:10.3390/polym13172871.

And has been presented at the 7th International Conference “CRETE 2021” on Industrial and Hazardous Waste Management

Vavouraki, A.I., Venieri, D., Komnitsas, K., **2021.** Properties of inorganic polymers based on waste concrete containing CuO and ZnO nanoparticles. 7th Int. Conf. Ind. Hazardous Waste Manage., Chania, Crete, July 27–30.

Abstract

The effect of copper oxide and zinc oxide nanoparticles (NPs) on the mechanical and thermal properties of ground waste concrete inorganic polymers (GWC IPs) has been investigated. NPs are added to GWC at loadings of 0.1, 0.5, 1, and 2% w/w. The phase composition and microstructure of NPs GWC IPs have also been examined using X-ray diffraction (XRD), Raman spectroscopy and scanning electron microscope (SEM/ EDS) techniques. Results show that the mechanical properties of GWC IPs are improved (23 MPa) due to addition of NPs (1% ZnO). In particular, GWC IPs in which 0.5% CuO and 1% ZnO NPs were embedded exhibited relatively improved compressive strength. The addition of NPs decreases the macroporosity and increases the mesoporosity of IPs matrix and decreases relatively the ability of IPs matrix to water absorption. The antimicrobial activity of GWC IPs doped with 0.5 and 1% CuO NPs against *E. coli* was also determined.

Keywords: Inorganic polymers; ground waste concrete; nanoparticles; copper oxide; zinc oxide; antibacterial activity

Περίληψη

Διερευνήθηκε η επίδραση των νανοσωματιδίων οξειδίου του χαλκού και οξειδίου του ψευδαργύρου (NPs) στις μηχανικές και θερμικές ιδιότητες των ανόργανων πολυμερών σκυροδέματος (GWC IPs). Τα NPs προστέθηκαν σε GWC ανόργανα απολυμερή με αναλογία 0.1, 0.5, 1 και 2% w/w. Εξετάστηκαν η σύσταση και η μικροδομή των NPs GWC IPs χρησιμοποιώντας τεχνικές περίθλασης ακτίνων X (XRD), φασματοσκοπίας Raman και ηλεκτρονικού μικροσκοπίου σάρωσης (SEM/ EDS). Τα αποτελέσματα έδειξαν ότι οι μηχανικές ιδιότητες των GWC IPs βελτιώνονται (23 MPa) λόγω της προσθήκης NPs (1% ZnO). Συγκεκριμένα, τα GWC IPs στα οποία ενσωματώθηκαν 0.5% CuO και 1% ZnO NPs παρουσίασαν σχετικά βελτιωμένη αντοχή σε θλίψη. Η προσθήκη NPs μειώνει το μακροπορώδες και αυξάνει το μεσοπορώδες των IPs και μειώνει σχετικά την ικανότητα της μήτρας IPs στην απορρόφηση νερού. Τέλος προσδιορίστηκε η αντιμικροβιακή δράση των GWC IPs με 0.5 και 1% CuO NPs έναντι του *E. coli*.

Λέξεις κλειδιά: Ανόργανα πολυμερή, απόβλητα σκυροδέματος, νανοσωματίδια, οξείδια χαλκού, οξείδια ψευδαργύρου, αντιμικροβιακή δράση

Aim of the study

Nanoparticles in inorganic polymer preparation is very limited. To the best of our knowledge this is the first attempt to use synthesized CuO and ZnO NPs embedded in ground waste concrete-based IPs. The aim of this study was to determine the effect of both synthetic CuO and ZnO NPs on physicochemical and thermal properties of GWC IPs. In particular the structural, mechanical, and thermal behavior of GWC IPs admixed with different concentrations of CuO and ZnO NPs (0.1 to 2%) was examined. The mechanical properties and microstructure of the produced IPs were determined through XRD, Raman, SEM/EDS, and TG/DTA analyses. The antibacterial potential of NPs GWC IPs was also investigated against Gram-negative Escherichia coli bacteria. Toward a better green construction technology GWC IPs binders are considered eco-friendly, non-hazard, cost effective, and more durable building materials that could be used in constructions, repair, and restoration cases [Nawaz et al., 2020; Shehata et al., 2021]. Additionally, possible utilization of IPs embedded with NPs with antibacterial activity may be considered for functional surface applications such as floors and walls in houses and hospital facilities and/or marine concrete structures.

1. Introduction

Due to rapid urbanization the increase in demand for engineering infrastructures, 20% of all greenhouse gas emissions is attributed to construction and also to maintenance of the built environment. The cement industry is responsible for c.a. 8% of global CO₂ emissions [Andrew, 2018]. Thus, it is of great environmental challenge in (partial) substituting cement as a raw material by using Portland cement clinker (PC) with supplementary cementitious materials or with non-clinker based cements such as recycled aggregates. Up to 20% substitution of virgin aggregates with concrete waste is not considered to lower the new concrete's properties and can be used for structural applications [Tam et al., 2018]. The main difficulty for recycling aggregates from concrete waste in new concrete is the low cost of raw materials and also, the processing costs of demolition wastes to secure high-quality material for recycling. The recent Circular Economy Package, launched by the European Commission introduces a new perspective on waste management policy-making through sustainability principles [EU, 2020]. Policy measures encompass taxes on raw materials, the encouragement of green public procurement, taxes for landfilling, and end-of-waste criteria, among others. Scrivener et al. [2018] stated that increasing the average level of PC substitution in cement to 40% could avoid up to 400 Mt CO₂ emissions globally each year.

Concrete is the second most widely used substance after water around the globe. Concrete is a composite material consisting of binding materials (i.e. Portland cement, lime) mixed with aggregates (i.e. sand, gravel etc.) and/ or chemical or mineral admixtures (i.e. fly ash) [Aïtcin, 2000] in water in specific proportions. Due to its large volume utilization in countless construction works from tower blocks to carparks cement production has considerably increased the last years contributing 5% of annual anthropogenic global CO₂ production. The high range of concrete applicability indirectly related to millions of tons of waste concrete generation every year around the world due to different reasons such as demolition and destruction of old structures and buildings due to natural causes i.e. earthquakes, removal of useless concrete from structures, buildings, road pavements etc. and also, due to concrete cube and cylinder testing, destructive methods of testing of existing structures [Ganiron, 2015]. Aggregates from construction and demolition wastes (CDWs) or precast concrete residues, seems to be a promising contribution towards the sustainability of the construction industry [Behera et al., 2014]. However low volumes of recycled CDWs is utilised as partial replacement aggregates in cement industry while the large part of waste concrete is still disposed in landfills [Phair, 2006].

Ground waste concrete (GWC) constitutes part of the debris of construction and demolition wastes (CDW) that are generated during the construction, renovation, and demolition of buildings, roads, and other engineering works. About 374 million tons of CDW were generated in 2016 making CDW the largest waste stream in the EU by weight [Mavridou et al., 2015]. In Greece CDW account for ca. 4 million tons per year [Eurostat, 2019a]. According to EUROSTAT study [EU-28, 2016] an overview of waste production divided by EU countries and industrial sectors is provided (Fig. 1.1). In 2016, the total waste generated in the EU-28 by all economic activities and households amounted to 2,538 million tons. In the EU-28, construction contributed 36.4% of the total in 2016, followed by mining and quarrying (25.3%), manufacturing (10.3%), waste and water services (10.0%), and households (8.5%). The data collected underline that Architecture, Engineering, Construction, and Owner (AECO) sector is responsible of 924 million tons of waste out of the total of 2,539 million tons.

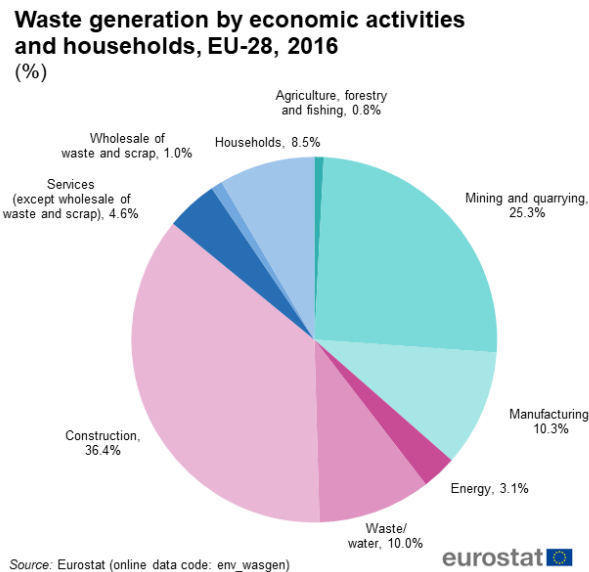


Figure 1.1: Waste generation by economic activities and households [EU-28, 2016].

The waste hierarchies for demolition and construction operations are shown in **Fig. 1.2**. Construction waste management should move increasingly towards the first of these options, using a framework governed by five key principles promoted by the European Union (EU): The proximity principle; Regional self sufficiency; the precautionary principle; the polluter pays; and best practicable environmental option. The reuse of building elements should evidently take priority over their recycling, if practicable, to help satisfy the first priority of waste prevention at source. Disposal of waste should be considered a last option, for materials that cannot be reused or recycled in the region. Unsorted loads of such waste may incur in a disposal penalty at landfills. Hazardous materials need to be disposed of correctly. Thus a way of waste management could also be upcycle (recycle) producing added-value products such as inorganic polymers.

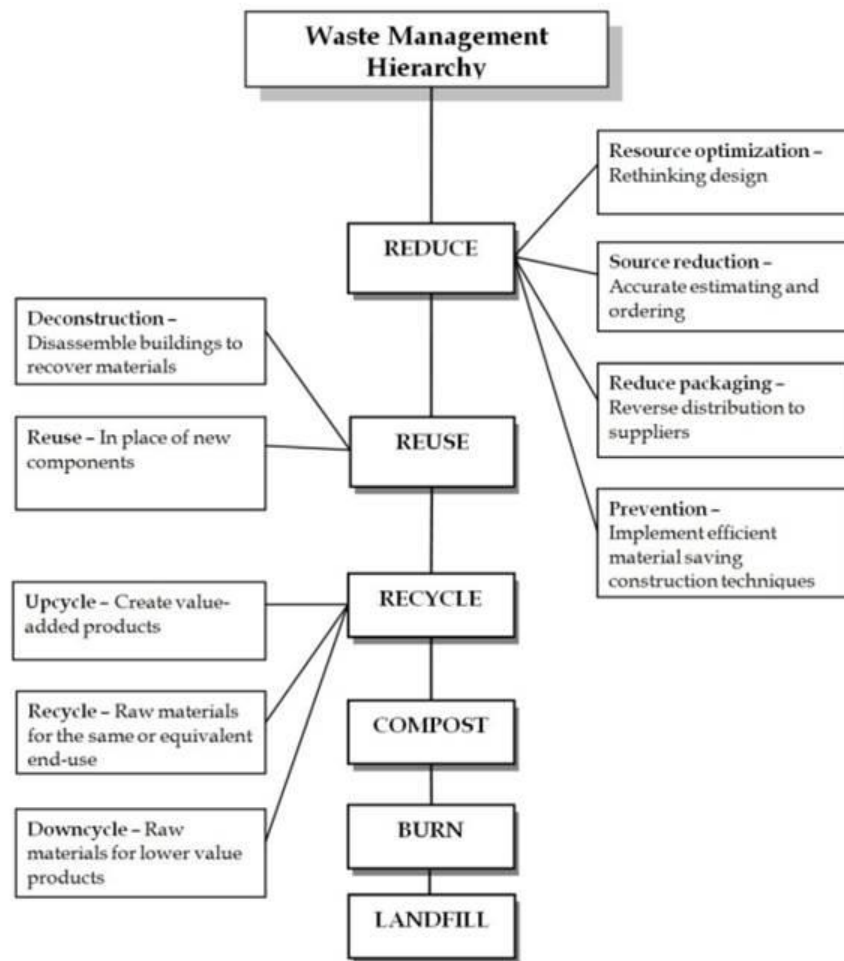


Figure 1.2: Hierarchies for demolition and construction operations [Couto & Couto, 2010].

In the EU according to the Circular Economy Action Plan construction and demolition is defined as a priority area among other sectors (plastics, food waste, critical raw materials, biomass and bio-based products) [EU, 2020]. Toward a circular economy the lifecycle of construction products may include preservation of resources and hence closing the loop. CDW management is of great significance providing environmental benefits involving waste prevention and/or less waste generation. In the framework of the recycling concept, the partial substitution of cement with alternative raw materials such as CDW may lead to significant constraints of CO₂ production in the future.

According to EU Action Plan for the Circular Economy 2016 (Fig. 1.3), the objective of a Circular economy is to maintain the value of resources in the economy for as long as possible bringing long-term benefits. Thus some of the risks related to the supply of raw materials could be alleviated boosting the European economy by up to 7% of Gross Domestic Product (GDP). The competitiveness of European businesses and should be increased by creating new business opportunities (re-use sector) and bringing about innovative products, technologies and services, thus creating new jobs in the EU. Outstanding and valuable benefits to the environment –less waste, less GHG emissions and other benefits, like better air and water and soil quality are anticipated.



Figure 1.3: A circular economic model to achieve sustainability and increase Europe’s competitiveness globally (**Circular economy, 2016**).

Circular economy. Closing the loop- An EU Action Plan for the Circular Economy, 2016. Available online: https://ec.europa.eu/environment/strategy/circular-economy-action-plan_en (accessed on 29 December 2021)

1.1 Inorganic polymers

Towards the mitigation of global warming and greenhouse gas emissions, construction industries need to adopt more sustainable practices including the use of eco-friendly construction materials. Valorization of concrete waste and metallurgical slags through alkali-activation appears to be a viable management option. A recent trend is the replacement of highly energy intensive product of ordinary Portland cement by alkali activated materials and inorganic polymer composites in concrete derived from recyclable waste materials and industrial by-products [Komnitsas & Zaharaki, 2007; Pacheco-Torgal et al., 2012; Mehta & Siddique, 2016; Mohajerani et al., 2019]. Inorganic polymers (IPs) are synthetic alkali aluminosilicate materials produced from the reaction of solid aluminosilicate-rich with a highly concentrated aqueous alkaline hydroxide (NaOH or KOH) and/ or sodium or potassium silicate solution, resulting into an amorphous to semi-crystalline polymeric structure [Davidovits, 1991].

Geopolymers are ceramic-like IPs produced at low temperature (<100 °C). They consist of chains or networks of mineral molecules linked with covalent bonds. Due to the geological origin of the minerals contained in the raw materials used, they called “geopolymer”. Initially the reactivity of calcined kaolinite, as an aluminosilicate oxide $\text{Si}_2\text{O}_5\text{Al}_2\text{O}_2$, metakaolin, was studied leading to the discovery of geopolymers 40 years ago.

Geopolymers compomises of aluminosilicate materials with three-dimensional amorphous microstructure. To synthesize geopolymer different mediums are used; alkaline mediums (Na^+ , K^+ , Li^+ , Ca^+ , etc.) and/ or acidic mediums (phosphoric acid, humic acid). Geopolymerization process in alkaline medium, occurs when the oxides of silicon and aluminium minerals or aluminosilicates reacts with

alkaline solution forming polymeric Si-O-Al bonds (silicon-oxo-aluminate, sialate). The structures are of poly(sialate) type (-Si-O-Al-O-), poly(sialate-siloxo) type (-Si-O-Al-O-Si-O-) and poly(sialate-disiloxo) type (-Si-O-Al-O-Si-O-Si-O-) as depicted in **Fig. 1.4** [Ng et al., 2018]. The network of sialate comprises of silicate (SiO_4) and aluminate (AlO_4) which is connected tetrahedrally by sharing an oxygen atom. Positives ions required in the framework cavities, balance the negative charge of aluminium ion in IV-fold coordination.

The empirical formula of poly(sialates) is $Mn[-(\text{SiO}_2)_z\text{-AlO}_2]n, w\text{H}_2\text{O}$, where M is a cation (Na^+ , K^+ , Ca^{2+}); n is the degree of polycondensation; z is 1, 2, 3

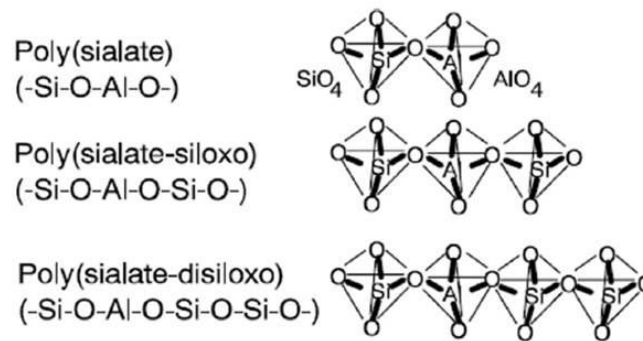


Figure 1.4: Poly(sialate) structures [Ng et al., 2018].

According to previous study [North & Swaddle, 2000] the molecular structure and polymeric character of IPs were described by NMR spectroscopy. The polymerization of oligo-sialates was proved to taking place faster (100 msec) than the polymerization of ortho-silicate. IPs comprise several molecular units such as silico-oxide (Na,K)-(-Si-O-Si-O-) for (Na,K)-poly(silicate) or (Na,K)-poly(siloxonate), silico-aluminate (Na,K)-(-Si-O-Al-O) for (Na,K)-poly(sialate), ferro-silico-aluminate (Na,K)- (-Fe-O-Si-O-Al-O-) or (Na,K)-poly(ferro-sialate), alumino-phosphate (-Al-O-P-O-) for poly(alumino-phosphate), formed in a geopolymerization process.

Five solute species depicted in **Fig. 1.5**:

- For Si: Al= 1: one ortho-sialate $(\text{OH})_3\text{-Si-O-Al}(\text{OH})_3$
- For Si: Al= 2: one linear ortho(sialate-siloxo) $(\text{OH})_3\text{-Si-O-Si}(\text{OH})_2\text{-O-Al}(\text{OH})_3$, one cycle ortho(sialate-siloxo)
- For Si: Al= 3: two cycles ortho(sialate-disiloxo)

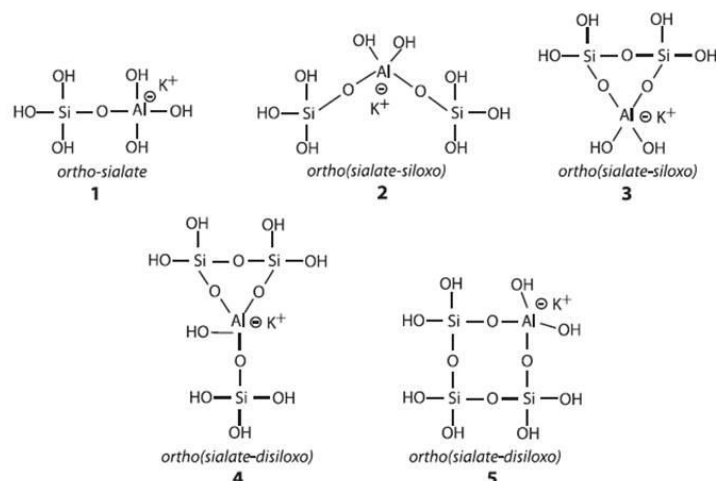


Figure 1.5: Five ortho-sialate oligomers isolated in KOH solutions [North & Swaddle, 2000].

According to the geopolymerization mechanism initiation of polycondensation of oligomers into small ribbon-like molecules occurs [Davidovits, 2017] involving several Si-OH groups together with H₂O molecules. It is referred to as sodium-alumino-silicate hydrate, NASH and potassium-alumino-silicate hydrate, KASH resulting into the final geopolymer structure. The poly(sialate) final structure consists of well-polymerized individual elementary nanoparticles of 5 to 40 nm in size.

The atomic ratio Si: Al governs the chemical, physical and mechanical properties of ceramic-like materials found in a wide variety of uses. Certain geopolymer applications are still in development whereas others are already industrialized and marketed. The following areas may be mentioned (Fig. 1.6) [Davidovits, 2018]:

- Si:Al=1: geopolymer ceramics and manufacturing techniques with low-CO₂ greenhouse gas emission
- Si: Al= 2: geopolymer cements and concretes with low-CO₂ greenhouse gas emission and low energy demand; treatment and containment of toxic, radioactive and nuclear waste and mine tailings
- Si: Al= 3: fire- and temperature-resistant compounds for the manufacture of prototypes and tooling
- Si: Al> 3: high-tech geopolymer resins and binders for paints, coatings and grouts resistant to corrosion and temperature; tooling for aluminum industry
- Si: Al> 20: high-tech composites made of carbon fibers and others, resistant to fire and heat for aeronautics and automotive, for the repair and reinforcement of civil engineering infrastructure

The wide variety of potential applications include fire-resistant materials, decorative stone artifacts, thermal insulation, low-tech building materials, low-energy ceramic tiles, refractory items, thermal shock refractories, biotechnology (materials for medical applications), foundry industry, cement and concretes, composites for infrastructure repair and reinforcement, high-tech composites for aircraft interior and automobiles, high-tech resin systems, radioactive and toxic waste containment, arts and decoration, cultural heritage, archaeology and history of sciences [Davidovits, 2018].

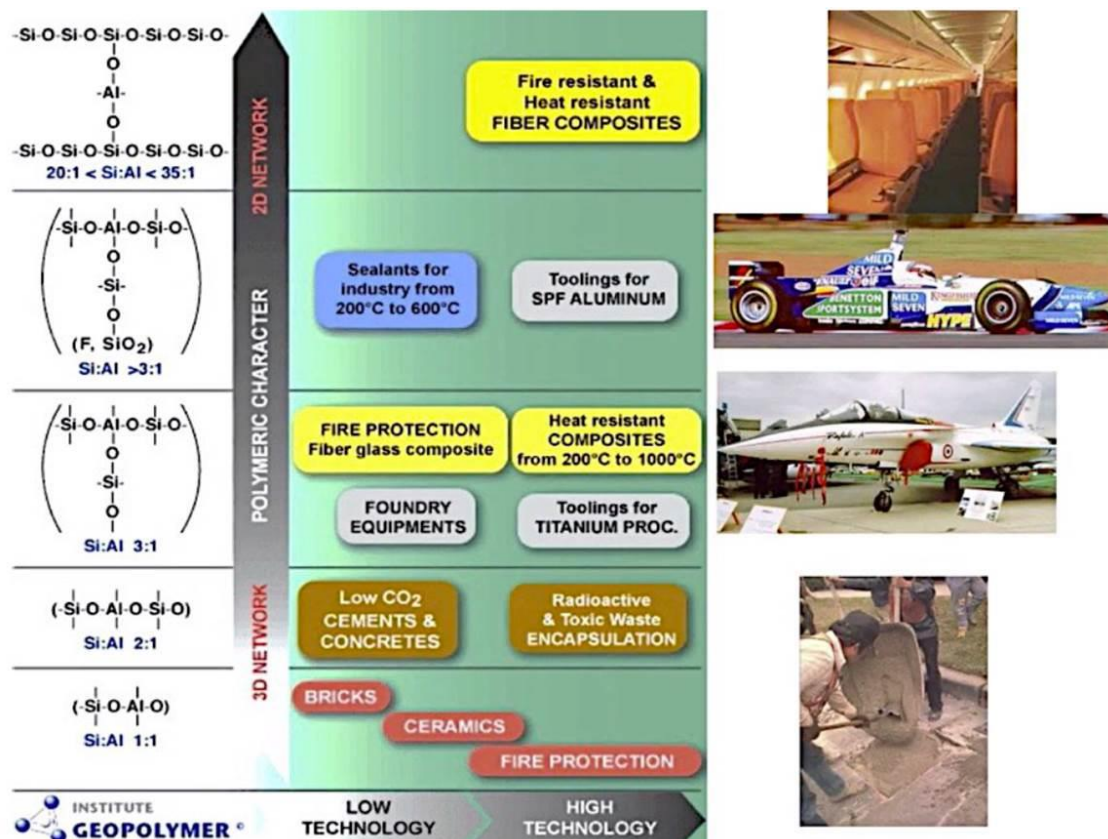


Figure 1.6: The atomic ratio Si: Al in the poly(sialate) structure determines the properties and application fields. A low Si: Al ratio (1,2,3) initiates a 3D-Network that is very rigid. A high Si: Al ratio (>15) results into linear polymeric structure of the geopolymeric material [Davidovits, 2018].

It is worth mentioning that geopolymers are polymers whereas Alkali-Activated Materials (AAM) are hydrates. Geopolymers are not a subset of AAM as the former are not a calcium hydrate alternative (no NASH, no KASH). They belong to two different and separate chemistry systems. AAM are hydrates/ precipitates comprising of monomers and/ or dimers. Alkali activation of materials comprises only the first step of geopolymerization. Geopolymers are true three-dimensional framework silico-aluminates with polymeric building units, (Na, K)-poly (sialate-siloxo) (Na, K)-(Si-O-Al-O-Si-O) [Davidovits, 2018].

Solubilization of Al-Si-rich wastes or by-products, including CDWs and metallurgical slags is possible for the exploitation of the production of inorganic polymers. Towards the scope of environmental sustainability inorganic polymer technology adaptation can succeed in both utilizing industrial wastes as added-value materials but also contributing to the decrease of CO₂ emissions [Komnitsas, 2011; Ma et al., 2018]. Numerous studies focus on the valorization of such materials demonstrating advantageous properties including high compressive strength, effective in acid and salt resistance [Bakharev, 2005; Komnitsas et al., 2007; Ariffin et al., 2013] lower shrinkage, resistance to high temperature firing [Zaharaki et al., 2016] and effective in heavy metal immobilisation compared with concrete-made with Portland cement [Komnitsas et al., 2013].

Despite large number of research studies on alkali activated materials and inorganic polymer binders incorporating industrial wastes or by-products limited research focus on valorization of recycling waste concrete displayed in the construction and demolition wastes. Due to the lack of aluminosilicate content in waste concrete matrix co-valorization is better applied for simultaneous treatment of different by-products, in which the aluminosilicate content can thereby be present giving the opportunity of synergistic and efficient management of solid wastes. Towards that concept different

researchers examined the production of inorganic polymers cements utilizing concrete incorporating brick, tiles [Komnitsas et al., 2015; Wong et al., 2018], marine sediments [Komnitsas, 2016] and/ or industrial wastes such as fly ash [Ahmari et al., 2012; Cristelo et al., 2018], metallurgical slags [Ariffin et al., 2013; Komnitsas et al., 2019; Komnitsas et al., 2020] as raw materials. In general alkali activated waste bricks and tiles exhibited higher compressive strength in comparison to waste concrete due to a combination of silica and alumina content in the initial raw materials. Alkali activated of solely concrete waste results into low compressive strength inorganic polymer binder. However co-utilization together with fly ash can increase the UCS up to 50% GWC content [Ahmari et al., 2012]. Beyond the mineralogy and the raw materials' composition namely the ratios of Si/Al and/ or Si/(Al+Ca) the amount of alkali solution and experimental conditions of alkali activation process such as curing temperature and, time and the additives are critical factors that affect mechanical performance of produced specimens [Zhuang et al., 2016].

Inorganic polymers (IPs) are considered as the third generation of concrete, since they are viable for the preparation of cements, mortars, and concrete with properties similar or higher than traditional materials used in constructions [Sotelo-Piña et al., 2018]. IPs have a lower carbon footprint compared to PC [Davidovits, 2015; Maddalena et al., 2018] IPs obtain good and prospective properties over the PC system with excellent mechanical properties, good chemical and fire resistance, low shrinkage, environmentally friendly nature, and long-term durability [Singh et al., 2015; Amran et al., 2020]. Previous studies focus on the valorization of CDW and/or industrial slags through inorganic polymerization [Komnitsa et al., 2015; Zaharaki et al., 2016; Komnitsas et al., 2019; Soutana et al., 2019; Vavouraki, 2020]. Various application potential of IPs including toxic waste immobilization, building, and high temperature-resistant materials have been recently extensively reviewed [Wu et al., 2019; Tan et al., 2020].

The addition of nanoparticles (NPs) is a way to develop and modify IPs properties. Among unique physical and chemical properties of NPs, their high surface area and nanoscale size are considered additional advantage [Khan et al., 2019]. Good absorbability, mechanical properties, optical activity, and chemical reactivity with high dispersibility in alkaline solutions make NPs suitable materials for different applications. Singh et al. [2018a] demonstrated that the incorporation of different NPs (carbon nanotubes, nano -SiO₂, -TiO₂) in IPs mortars/concrete exhibited significant potential to be used as an effective building material in civil engineering field applications. In a recent review Rashad [2019] underlined the effect of NPs namely nano-SiO₂, -TiO₂ -Al₂O₃, -clay, and -silica waste into different IPs matrices. Specifically, NPs' unique properties lead to their use as filler in IPs. There is an optimum concentration of NPs added in different-based IPs (i.e., fly ash-, metakaolin-, and slag- based IPs) that contribute to a better mechanical performance due to physical filler effect of NPs [Deb et al., 2016; Guzmán-Aponte et al., 2017; Ramezani-pour & Moeini, 2018; Zailan et al., 2019]. Thus, a relatively compact microstructure of IPs is achieved. The inclusion of NPs densifies the microstructure of IPs composites producing high mechanical strength. Due to the formation of a dense NPs-embedded-matrix of IPs gel interconnectivity of micropores is hindered [Jindal & Sharma, 2020]. An increase of scientific interest concerns the synthesis of high-quality IPs with better mechanical, structural, and thermal properties and NPs could be used for that purpose [Xie & Fang, 2019; Liu et al., 2020]. Nonetheless, a relatively modest number of studies appear to elucidate the incorporation of CuO and ZnO NPs into IPs.

1.2 CuO and ZnO nanoparticles and inorganic polymers

CuO and ZnO NPs (and/or nanofluids) are among the most commercialized metal-based NPs. They are considered semiconductor materials for various applications with technological perspectives (energy conversion and, storage, solar collectors) [Janáky et al., 2015; Farhana et al., 2019] to environmental remediation acquiring antimicrobial properties, (photo)catalytic potential, removal of pollutants dyes, and heavy metal ion sensing [Chang et al., 2012; Singh et al., 2018b]. For cement -based materials

NPs accelerate the hydration of cement, decrease the porosity, and improve the pore structure of concrete [Konsta-Gdoutos, 2014; Mendes et al., 2015; Du et al., 2019]. CuO and ZnO NPs have already been suggested for improving physicochemical properties of cement [Rashad, 2013; Shafeek et al., 2020] and also operating as antibacterial cement admixtures for the production of cement -based composites [Sikora et al., 2018].

Recently, concrete and coatings incorporated with NPs have been proposed with novel functionalities such as self-protection and anti-corrosion ability and also, for prevention and control of biogenic deterioration of concrete [Noeiaghahi et al., 2017]. IP mortars are currently considered as being more environmentally friendly materials and may be a favorable contender to Portland cement concrete. Hence, it is of great research interest to examine IPs composites with embedded -NPs as antimicrobial agents. The addition of nanosilver improved the mechanical strength, durability, and antibacterial properties of Ag-IPs composites [Adak, 2015; Armayani & Pratama, 2017; Cerna et al., 2019]. Additionally, CuO and ZnO NPs can be included as reinforcement for IPs pastes [Qadry & Kharisma, 2019; Zidi et al., 2020] and also, generating antibacterial IPs surfaces [Nur & Sari, 2017; Gutiérrez et al., 2020].

2. Materials & methods

2.1 Synthesis of CuO and ZnO nanoparticles

Dispersed CuO and ZnO NPs were obtained by co-precipitation of hydroxycarbonates from corresponding crystalline solids of $\text{Cu}(\text{NO}_3)_2 \cdot 3\text{H}_2\text{O}$ (Sigma-Aldrich, Burlington, MA, USA) and/or $\text{Zn}(\text{NO}_3)_2 \cdot 6\text{H}_2\text{O}$ (Alpha Aesar) and NaHCO_3 (Alpha Aesar, Stoughton, MA, USA). The latter solution was added drop-wise in metal nitrate solutions under vigorous (magnetic bar) stirring rate (c.a. 300 rpm) at 65 °C for 3 h. Following filtration (membrane filters 0.45 μm cellulose acetate), the synthesized hydroxycarbonates powders were dried overnight at 80 °C (Jeio Tech, Des Plaines, IL, USA, ON-02G) and calcined in a pre-heated oven (N-8L SELECTA) at 350 °C (at a heating rate 10 °C \cdot min $^{-1}$) for 5 h to obtain the corresponding metal oxides. CuO and ZnO NPs were placed in distilled deionized water (10 mg \cdot L $^{-1}$) and subjected to sonification for 5 min to reduce agglomeration before characterization. NPs were characterized by XRD, BET, and SEM/EDS in order to determine phases, surface area, size, and morphology. Synthesis of CuO and ZnO NPs was previously reported by **Carbone et al. [2017]**.

2.2 Preparation of inorganic polymers

Ground waste concrete (GWC) was obtained from samples used for educational purposes at the Applied Mechanics Laboratory (School of Architecture, Technical University of Crete) and was pulverized in a Sepor type rod mill. A schematic diagram of the process used in this study is depicted in **Fig. 2.1**. GWC IPs were synthesized after alkaline activation of GWC with sodium hydroxide (NaOH 8 M) and sodium silicate solutions (Na_2SiO_3 : 27% SiO_2 , 8% Na_2O , mean values, Merck, Germany). The ratio of liquid to solid was 0.3 and the ratio of NaOH to Na_2SiO_3 solution was 0.9. The casting of the produced pastes lasted 3 h and, pastes were heated at 80 °C for 24 h, followed by curing for 7 days. Details of the experimental procedure and methodology of alkali-activated polymerization are described in a previous study [**Vavouraki, 2020**]. At similar conditions GWC IPs embedded with CuO and/or ZnO nanoparticles were prepared at loadings of 0.1%, 0.5%, 1%, and 2% NPs.

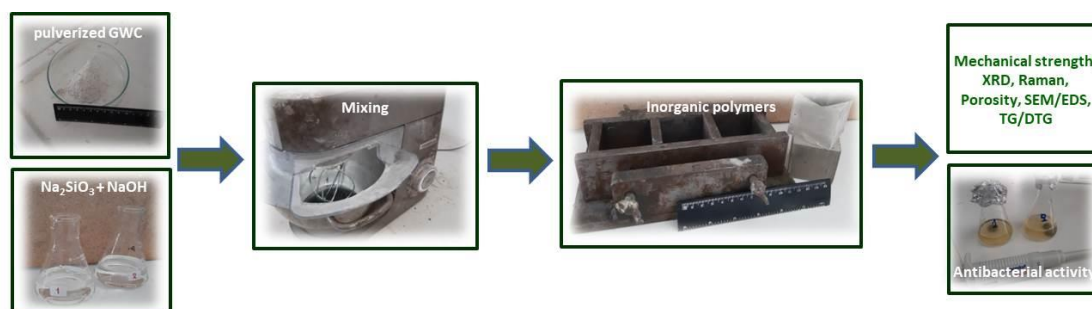


Figure 2.1: Schematic diagram of the process for the production of NPs GWC IPs following characterization analysis.

2.3 Structure analysis and characterization

The composition of the GWC raw material was determined by XRF analysis (XRF-EDS, Bruker-AXS S2 Range type, and SPECTRO X-LabPro, USA). MATEST C123N load frame was used for the determination of uniaxial compressive strength of GWC IPs embedded with NPs. For the analysis of micro/nanostructure, morphology, and phase/surface elemental compositions of the produced IPs XRD, Raman, and SEM/EDS analyses were also carried out. Additionally analysis of BET, mercury intrusion porosimetry, and TGA were also performed. According to Archimedes principle the physical properties of the selected IPs were also determined.

For XRD analysis the D8-Advance Bruker instrument, using Cu-K α 1 radiation at 40 kV and 40 mA, recorded at 20° to 80° (2 θ range), with a 0.02° step size was used. DIFFRACplus EVA[®] software

Bruker-AXS based on the ICDD Powder Diffraction File was used for the identification of crystalline phases.

Raman spectra were recorded on a T-64000 (Jobin Yvon-Horiba, UK) micro-Raman system equipped with a 2D-CCD Symphony II detector. The excitation wavelength (514.5 nm) was provided by a DPSS laser (Cobolt Fandango TMISO laser). The laser power on the sample was maintained at 1.2 mW and was focused on the samples by a 50× microscope objective. The Raman spectra were recorded in the region of 160-2200 cm^{-1} .

A field emission scanning electron microscope, SEM (FE-SEM, Leo Supra 35VP, Germany) equipped with an energy dispersive X-ray (EDX, QUANTA 200, Bruker AXS) with an accelerating voltage of 20 kV was used for morphological examination. In order to improve image quality and obtain high resolution images, the samples selected for SEM analysis, were coated with gold using a sputter coater.

The physical properties of GWC IPs embedded with NPs were determined according to the Archimedes principle as described in a previous study [16]. Thus, the apparent porosity and relative density and also, water absorption of samples were determined.

A NOVA Surface Area Analyzer (Quantachrome instruments, Boynton Beach, FL, USA) using nitrogen as the adsorbent gas at 77 K was used for the analysis of the Brunauer-Emmet-Teller (BET) surface area and pore analysis. Prior to these measurements, samples (about 1 g) were degassed (at 473 K overnight under vacuum). The relative pressure range was 0.05 to 0.3 for the gas adsorption analysis for the determination of the total specific area. According to the isotherm data of the BET method the surface area measurements were calculated with an accuracy of 10% and using t-plot analysis the total pore volume of the samples was calculated. The average pore size was obtained according to the Barrett-Joyner-Halenda (BJH) method.

Mercury intrusion porosimetry (Micromeritics Autopore IV 9400 porosimeter, Atlanta, GA, USA) was used to examine the macroporosity and to determine the open porosity and bulk density of selected samples.

Differential thermal analysis was carried out with TG/DTG analyzer (Model TGA 6 Perkin Elmer, Waltham, MA, USA). A maximum temperature of 900 °C was performed for the thermogravimetric analysis at a heating rate of 10 °C·min⁻¹ and 80 mL·min⁻¹ flow rate of nitrogen atmosphere.

2.4 Antibacterial activity

Varied amounts of CuO and ZnO-NPs (0.5, 1, and 2%) were tested against a reference strain of *Escherichia coli* (DSM 498) regarding the antibacterial properties of GWC IPs. Samples were prepared in the form of disks (Ø 20 mm), designated as Cu0.5, Cu1, Zn1, Zn2 for 0.5%, 1%, and 2% doped GWC IPs. Due to high alkalinity of alkali-activated samples (c.a. pH 12) disks of GWC IPs with NPs were Prior to antibacterial study, immersion of samples in HCl 0.1 M twice (with fresh solution) for 1 h was performed.

Tests of bacterial inactivation were performed in nutrient broth (LABM) with a bacterial concentration of 10⁵ CFU/ mL. In particular samples were added in 6 mL of liquid culture, which was further diluted with NaCl (0.7% w/v) to a final volume of 50 mL, in order to obtain the desired bacterial concentration (10⁵ CFU/mL). Incubation of all mixtures occurred at 37 °C for 24 h. Past the time of the incubation period, the optical density of each liquid culture was measured (at 600 nm) and viable counts were performed applying the spread plate technique and using LABM. Total of 200 µL of each liquid culture was spread onto nutrient agar plates, followed by incubation (at 37 °C for 24 h). The evaluation of bacterial reduction was performed through colony counting. Additionally, uncoated beads were tested as control samples in order to investigate any effect on bacterial growth. The antimicrobial potential of NPs GWC IPs (in disks) was expressed as *E. coli* growth per sample weight and area (*E. coli*/ kg sample/ m²).

Metal ion concentration of copper and/ or zinc in the same liquid culture that was used for bacterial growth, was measured by inductively coupled plasma mass spectrometry (ICP-MS, Agilent Technologies, Santa Clara, CA, USA 7500cx).

3. Results & Discussion

3.1 Characterization of nanoparticles

Fig. 3.1 shows the powder XRD patterns of CuO and ZnO NPs and the observed peaks were in excellent agreement with the standards (JCPDS Pdf No. 44–706 and 36–1451 for tenorite, CuO and zincite, ZnO, respectively). The particles were well crystallized.

The average nanocrystallite size of NPs was estimated by using Deybe-Scherrer equation [Cullity, 2002]:

$$D = K \frac{\lambda}{B \cos \theta} \quad (1)$$

where, λ is the X-ray wavelength (0.154 nm), K is Scherrer constant (0.9), and B is the full width at half maximum intensity (FWHM in rad); θ is the Bragg angle (in rad).

The size of the obtained CuO and ZnO NPs is calculated 20 and 16 nm, respectively. BET analysis determined the surface area of CuO and ZnO NPs that were 24.6 and 37.8 m²·g⁻¹, respectively in agreement with previous study [Carbone et al., 2017].

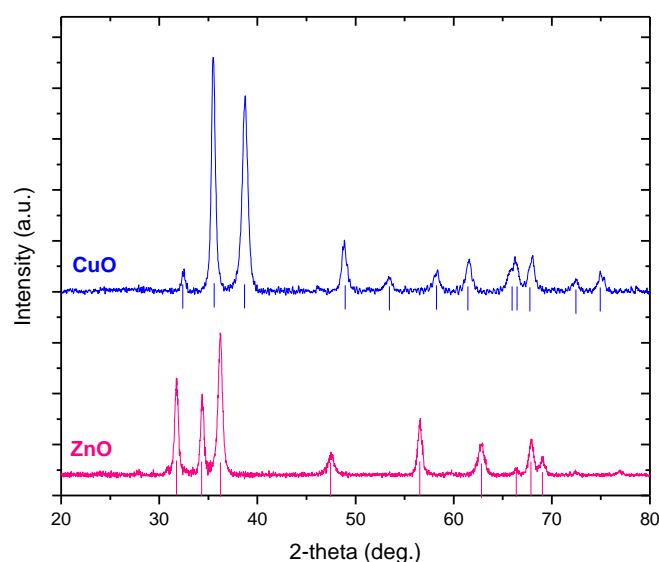


Figure 3.1: XRD patterns of CuO and ZnO NPs; straight lines indicate the match to the reference patterns of CuO and ZnO.

The morphology and the size of the produced CuO and ZnO nanoparticles were investigated by SEM/EDS (**Fig. 3.2**). Spherical assemblies as (agglomerated) NPs aggregates were observed. CuO NPs formed platy cluster (like dandelion) (**Fig. 3.2a,b**) while ZnO NPs have the shape of faceted crystals (**Fig. 3.2c,d**), as previously reported [Carbone et al., 2017; Jabbar et al., 2016; Dörner et al., 2019]. The size of synthesized CuO and ZnO were less than 200 and 100 nm, respectively and higher than the size of NPs determined by XRD. Agglomeration of NPs was observed despite sonication and thus, it was difficult to obtain accurate size measurements. Possibly high size of particles may be due to the fact that very small portion of the sample was examined by SEM analysis. Differences in average size obtained by XRD and SEM analysis have been previously reported [Geetha et al., 2016].

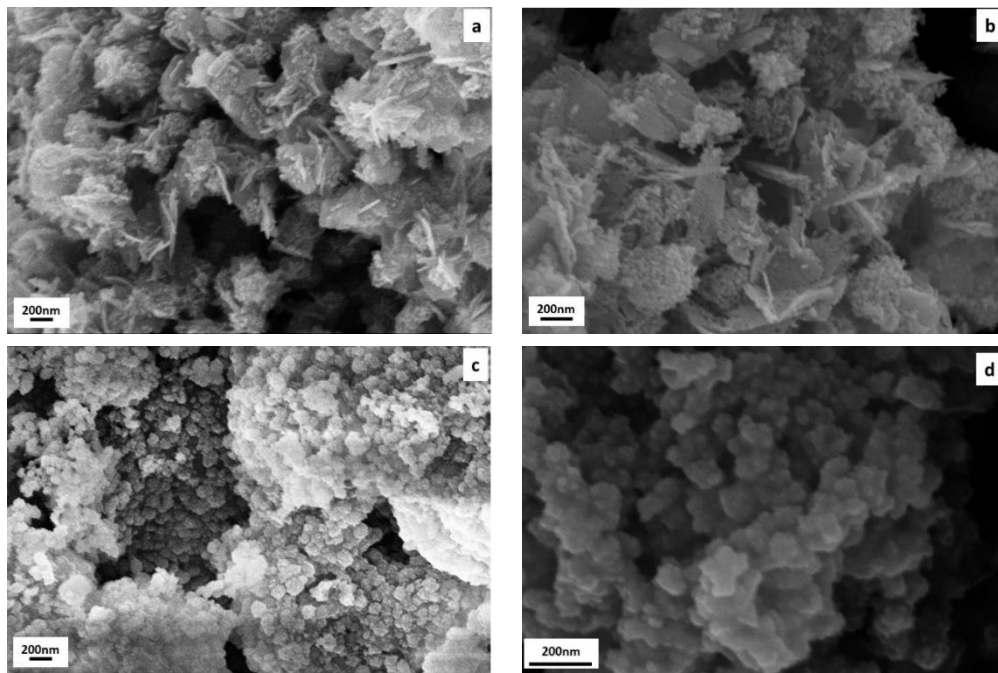


Figure 3.2. SEM images of (a,b) CuO and (c,d) ZnO NPs.

3.2 Characterization of inorganic polymers from Ground Waste Concrete with nanoparticles

Table 3.1 presents the elemental oxide composition analysis of raw material of ground-waste concrete (GWC) by oxides, according to XRF analysis. GWC is a Ca-rich material with low amounts of SiO₂ (3.96%) and Al₂O₃ (0.99%).

Table 3.1: Chemical analysis of ground-waste concrete (GWC) (% weight).

Oxides/ Material	SiO ₂	Al ₂ O ₃	CaO	Na ₂ O	Fe ₂ O ₃	MgO	K ₂ O	TiO ₂	MnO	P ₂ O ₅	SO ₃	SrO	* LOI
GWC	3.96	0.99	54.43	1.80	0.51	1.95	0.07	0.05	0.01	0.04	0.46	0.13	35.05

* LOI stands for loss on ignition at 1050 °C for 4 h.

3.2.1 Mechanical strength

The compressive strength of GWC IPs embedded with varied amounts of CuO and ZnO NPs (0.1 to 2%) was measured (**Fig. 3.3**). GWC IPs specimens have low compressive strength. Despite the fact that the SiO₂ to Al₂O₃ molar ratio is high in the initial paste (6.8) both molar ratios of SiO₂ to CaO and SiO₂ to (Al₂O₃ + CaO) are quite low (0.07). Thus, limited alkali activation is expected with few dissolved Si and Al ions for aluminosilicate bonding [**Vavouraki, 2020**]. 1% ZnO NPs GWC IPs had relatively higher compressive strength (23 MPa) compared to GWC IPs with and without CuO NPs. The compressive strength decreased at high amount of ZnO (2%) added in GWC IPs.

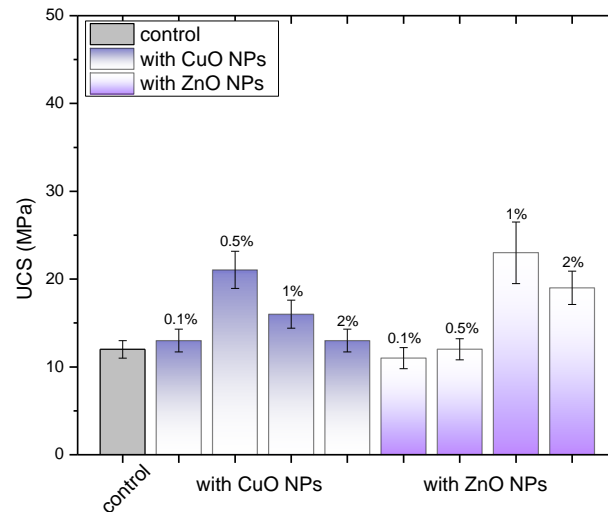


Figure 3.3: Compressive strength of CuO and ZnO NPs blended GWC IPs specimens (control: GWC IPs). Replicates of two IPs specimens (~10% standard error).

Previous studies investigated the effect of different NPs on the mechanical properties of IPs. The incorporation of 0.5% ZnO NPs and 2% Al₂O₃ NPs (of particle size of 60 nm and 300–500 nm) increased compressive strength of metakaolin-based IPs by 26% and 30%, respectively [Zidi et al., 2019, 2020]. Metakaolin geopolymer CuO-NPs composites gained improved flexural strength [43]. Silver (4 nm)-silica (20–40 nm) nano-composite-modified fly-ash-based geopolymer mortars had higher compressive strength compared to conventional (OPC) cement mortar [40]. The inclusion of nano-silica from 0 to 3% in the OPC and GGBFS blended IPs mortars increased compressive strength by 40 to 64% as compared to the corresponding control mixes [Deb et al., 2016].

3.2.2 XRD analysis

Fig. 3.4 shows the XRD patterns of CuO/ ZnO NPs and GWC IPs (control) with different amounts of CuO/ZnO NPs added. The presence of the main crystalline phases calcite and dolomite in GWC was identified (JCPDS Pdf No. 5–586 and 36–426 for calcite, CaCO₃ and dolomite, CaMg(CO₃)₂, respectively). The spectra exhibit intense peaks at 29.4° (2θ) corresponding to calcite. Limited amorphicity is indicated as no obvious hump is shown in the XRD patterns; thus, limited aluminosilicate gel is formed during geopolymerization justifying the low strength of GWC IPs. A small shift to higher angles is observed when adding NPs. This can probably be attributed to an interaction with the freely dissolved species [Zidi et al., 2020].

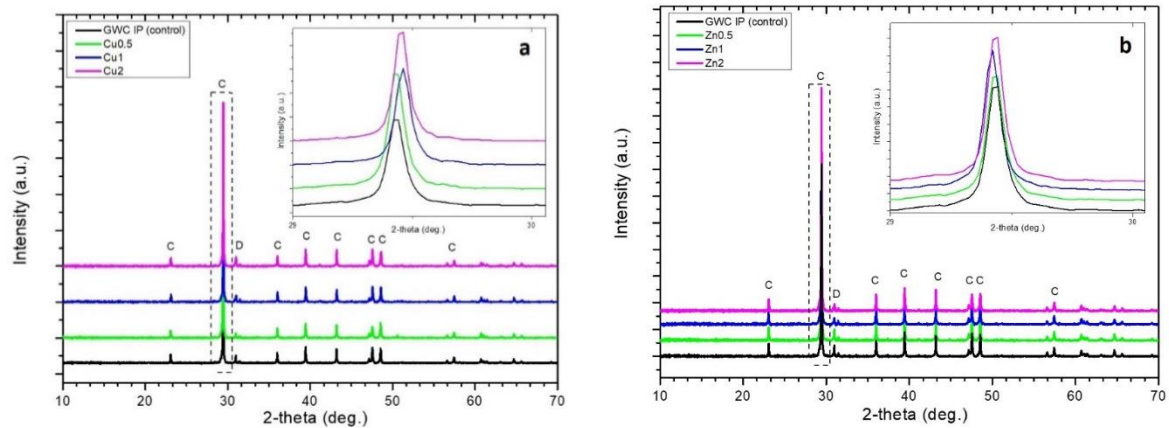


Figure 3.4: Powder X-ray diffraction patterns of GWC IPs (control) embedded with different amounts (0.5, 1%, and 2%) of (a) CuO and (b) ZnO NPs; C: calcite; D: dolomite depict the match to the reference pattern of calcite, CaCO_3 .

3.2.3 Raman analysis

Fig. 3.5 shows the Raman spectra of GWC IPs embedded with CuO and ZnO NPs. The characteristic vibrational signature of the calcite-type spectrum is present corresponding to symmetric stretching of CO_3 group at 1084 cm^{-1} and ν_4 symmetric bending mode at 711 cm^{-1} , and also the band at 280 cm^{-1} attributed to external vibrational modes of the CO_3 groups that involve relative translations between the cation and anionic group [Sun et al., 2014; Kosor et al., 2016]. Due to poor aluminosilicate content of raw material, GWC low strength of GWC IPs is anticipated, thus inorganic polymerization is limited [Vavouraki, 2020]. Vibrational frequencies of silicate species for Raman spectroscopy, typically found in aluminosilicate-matrix-IPs have been previously reported [Arnoult et al., 2018]. The asymmetric stretching vibrations of Si-O-Si or Al-O-Si was assigned at the $1050\text{--}1100\text{ cm}^{-1}$ region. In this study the main band was centered at 1084 cm^{-1} that may hinder limited vibrations of Si-O-Si and Si-O-Al linkages. The broadening of the 1084 cm^{-1} band and its shift to a slightly higher wavenumber may suggest formation of a differently structured material that is associated with limited geopolymerization and/or NPs addition into IPs matrix [Kosor et al., 2016]. The incorporation of nano-ZnO into the geopolymer matrix may be confirmed by a small shift of the intense peak. There is neither evidence of CuO or ZnO Raman signatures nor new functional group after the incorporation of CuO/ZnO NPs implying that only a physical interaction occurred between NPs and IPs matrix [Zidi et al., 2020].

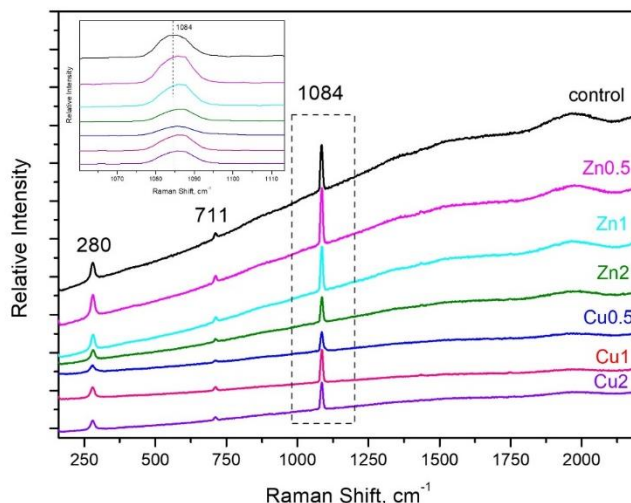


Figure 3.5: Raman spectra of GWC IP (control) embedded with different amounts (0.5 to 2%) of CuO and ZnO NPs; focused area at 1084 cm^{-1} .

3.2.4 SEM/ EDS analysis

Fig. 3.6 shows the scanning electron microscopy (SEM) images of GWC IPs embedded with 0.5% CuO NPs and 2% ZnO NPs. GWC IPs (control) have a porous structure with non-reacted particles (**Fig. 3.6a1**). Along the step edges of calcite (as identified in XRD analysis) there is limited gel formation (**Fig. 3.6a2**). Incorporation of CuO (**Fig. 3.6b1,b2**) and ZnO NPs (**Fig. 3.6c1,c2**) improved the homogeneity of GWC IPs matrix, forming a denser structure. This may be attributed to the filling of the matrix voids. Similar observations have been reported in previous studies [Deb et al., 2016; Zidi et al., 2020]. NPs may act as fillers in alkali-activated materials improving particle packing with reduced porosity and increased compressive strength.

The chemical constituents present in GWC IPs were identified by EDS analysis. The elemental composition of GWC IPs embedded with 0.5% CuO and 2% ZnO NPs are shown (**Fig. 3.6a3, b3, c3**). The presence of O, Ca, Si, Na, Mg, Al, K, and relatively low amounts of Cu and/or Zn was revealed (**Table 3.2**). Due to the gold coating process gold was also detected. Similar compositional analysis within samples indicate that limited gel formation was not hampered by the addition of NPs and the latter coexist in the structure of the GWC IP matrix. Comparable observations were obtained following the addition of titanium oxide particles into metakaolin-based IPs [Guzmán-Aponte et al., 2017].

Due to the addition of NPs into GWC IPs matrix during the preparation of the samples copper and zinc in GWC IPs was identified. Copper in GWC IPs (0.66% Cu or 0.41% CuO) is in good correlation with the initial content (0.5% CuO) added during the geopolymerization process. However, this was not the case for zinc (just 0.03% Zn or 0.04% ZnO compared to 2% ZnO initially). This may be due to the fact that the main sodium and zinc peaks overlap in EDS spectra.

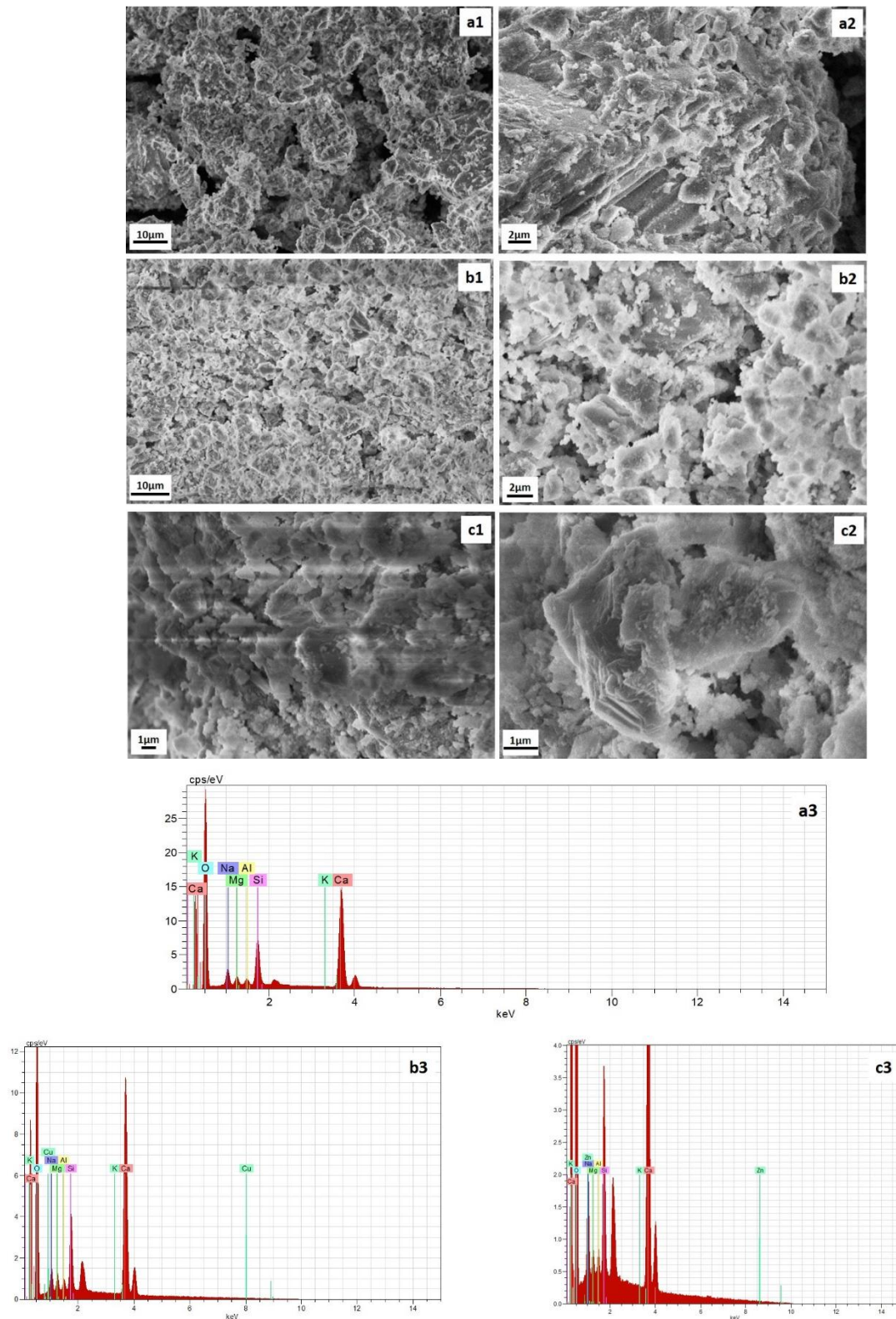


Figure 3.6: SEM images of (a1), (a2) GWC IPs (control); (b1), (b2) with 0.5% CuO NPs and, (c1), (c2) with 1% ZnO NPs; and (a3), (b3), (c3) EDS analysis.

Table 3.2: Elemental composition for GWC IPs embedded with 0.5% CuO and 2% ZnO NPs.

Sample Element	GWC IPs		Cu0.5		Zn2	
	Weight %	Atomic %	Weight %	Atomic %	Weight %	Atomic %
Ca	26.91	13.60	22.75	10.92	15.85	7.39
Si	5.88	4.24	4.44	3.04	5.48	3.65
Na	3.36	2.97	2.62	2.19	4.05	3.30
Mg	1.30	1.08	1.33	1.05	1.59	1.23
Al	0.83	0.62	0.76	0.54	1.35	0.94
K	0.20	0.10	0.30	0.15	0.34	0.16
Cu	n.d.	n.d.	0.66	0.20	n.d.	n.d.
Zn	n.d.	n.d.	-	n.d.	0.03	0.01
O	61.12	77.39	68.12	81.91	71.35	83.32
Total	99.6	100	100.98	100	100.04	100

3.2.5 Pores, water absorption, sorptivity

Fig. 3.7 shows the density and water absorption of GWC IPs with different amounts of NPs. GWC IPs with 0.5% CuO NPs and 1% ZnO NPs exhibit a relative density increase and water absorption reduction. The porosity results are in agreement with the compressive strength results following the addition of NPs. Beyond that amount of NPs in GWC IPs resulted in a decrease of density and increase of water absorption.

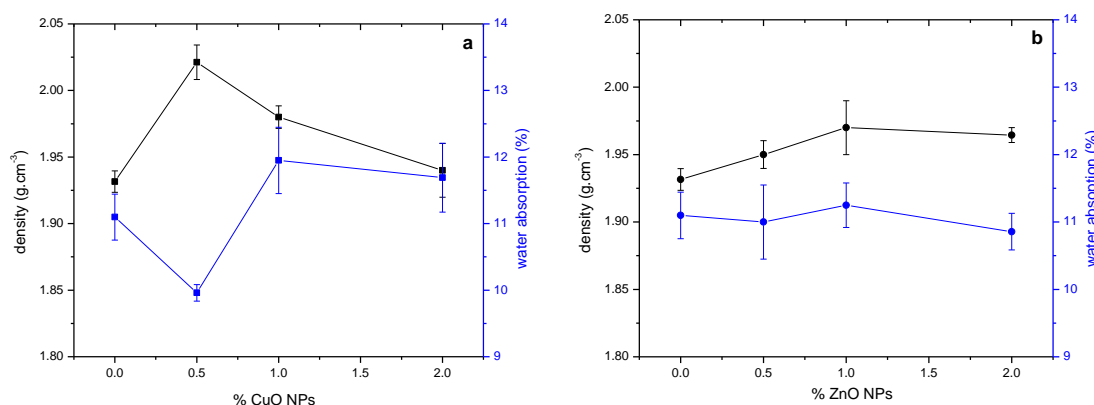


Figure 3.7: Density and water absorption of GWC IPs with different amounts of (a) CuO and (b) ZnO NPs.

Table 3.3 shows the physical characteristics of GWC IPs, namely specific surface area; total pore volume and average pore diameter in the presence of CuO and ZnO NPs. The average pore size obtained for GWC IPs is 87 Å; thus, it is classified as predominantly mesoporous material (mesoporosity range 45 to 500 Å). The medium pore volume and surface area for the GWC IPs indicate that IPs matrix is relatively dense with relative low permeability and relative high durability [Niveditha et al., 2020]. The incorporation of NPs into GWC IPs resulted into marginal differences in specific surface area and pore volume measurements. However, the average pore diameter (mesoporosity) of GWC IPs matrix embedded with NPs was increased by 42% (from 87.5 to 125 Å, mean value). This is an important result that correlates with compressive strength data (**Fig. 3.3**). The addition of NPs into GWC IPs matrix resulted into the augmentation of the mesoporosity of matrix and thus an increase of compressive strength of the matrix was expected. In principle, mesopores represent the voids between the IPs phases, while micropores primarily are within the gel network [Gunasekara et al., 2019]. The gel fills the cracks/voids between unreacted GWC particles during alkali-activation process, the pore space in the IPs matrix is limited, thus refining the size of the pores. In this study, mesoporosity of IPs matrix was increased by the addition of NPs.

Table 3.3: Physical characteristics of GWC IPs synthesized with various amounts of CuO and/or ZnO replacements.

Sample No.	Specific Surface Area, $\text{m}^2 \cdot \text{g}^{-1}$	Total Pore Volume, TPV, $\text{mm}^3 \cdot \text{g}^{-1}$	Average Pore Diameter, APD, \AA
Control	7.7	17	87.5
Cu0.5	6.5	20	124.6
Cu1	5.8	19	128.6
Cu2	8.1	26	129
Zn0.5	6.6	20	123
Zn1	8.0	22	108
Zn2	6.5	22	126

3.2.6 Hg-porosimetry analysis

Mercury intrusion porosimetry was performed for selected samples of 0.5% CuO NPs and 1% ZnO NPs GWC IPs and pore size distribution curves were defined (**Fig. 3.8**) and compared to GWC IPs (control; without NPs). The addition of NPs affected the porosity and pore distribution of IPs by increasing the number of small pores. The pore size distribution of GWC IPs (control) presented only one peak around 1 μm (range of capillary pores). The addition of 0.5% CuO and 1% ZnO NPs resulted in a shift to lower pore size (0.7 and 0.2 μm , respectively) compared to control. That is possibly due to the extent of filling the voids of GWC IPs. The mercury intrusion volume (area under the curve) was comparable for the control and 0.5% CuO NPs GWC IPs. However, this was not the case for 1% ZnO NPs GWC IPs. Total intrusion volume was lower due to better void filling effect of ZnO NPs compared to CuO NPs. In agreement with compressive strength results (**Fig. 3.3**), the lower the pore size of GWC IPs with 1% ZnO the higher the compressive strength. Poor development of IPs gel was observed during SEM/ EDS (**Fig. 3.6b,6c**), thus capillary pores are possibly formed by the space between unreacted GWC particles.

The average pore diameter of the selected samples was decreased from 0.125 μm to 0.111 μm and 0.093 μm (**Table 3.4**) as also shown by the porosity measurements of GWC IPs (from 26.5 to 18.5 and 23.5%, for 0.5% CuO and 1% ZnO NPs GWC IPs, respectively). In general, the presence of macropores that are larger than 0.2 μm is characteristic of less reacted IPs (as in our study). The macropores fill the gaps between unreacted GWC particles [**Gunasekara et al., 2019**]. Large capillary pores (>0.1 μm) initially found in the GWC IPs (control) became middle capillary pores (within 0.05–0.1 μm) for GWC IPs with CuO NPs. NPs filled the pores of IPs, as already confirmed by SEM captures.

The porosity decreased proportionally while increasing the mechanical strength (in agreement with mechanical strength data). The porosity reduction by including an appropriate amount of NPs could be relevant to IPs' pore structure by the filling effect [**Rashad, 2019**]. The addition of NPs improved microstructure of IPs possibly by chemical contribution of NPs through their high reactivity and their high specific surface area and also, the ability of unreacted NPs to fill IPs voids [**Ramezani pour & Moeini, 2018**]. Pore size is inversely proportional to the cross-linking density. Bulk density is defined as the total mass divided by the total volume (particles plus voids) [**Aredes et al., 2015**]. Therefore a decrease in the pore volume results into an increase in the bulk (or apparent) density. For 1% ZnO NPs GWC IPs high value of bulk (or apparent) density (2.09 and 2.74 $\text{g} \cdot \text{mL}^{-1}$ respectively) was obtained with a low value of void volume. IPs with high density generally result in high strength and a lower amount of voids and porosity. IPs with small voids show low (water and soluble elements) permeability [**Galiano et al., 2016**]. Specific surface area (7 $\text{m}^2 \cdot \text{g}^{-1}$, mean value) obtained by BET method is in a good agreement with the area measured by Hg porosimetry (5.2 $\text{m}^2 \cdot \text{g}^{-1}$, mean value) [**Lowell & Shields, 1991**].

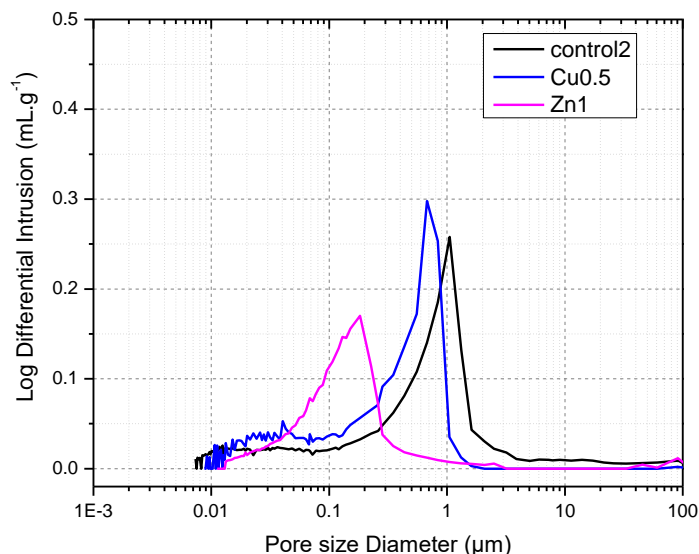


Figure 3.8: Pore size distribution (intrusion log differential, $\text{mL}\cdot\text{g}^{-1}$ vs. pore size diameter, μm) of selected samples of GWC IPs (control) with 0.5% CuO and 1% ZnO NPs.

Table 3.4: Mercury intrusion porosimetry (MIP) analysis.

	Control	Cu0.5	Zn1
Total Pore Area, $\text{m}^2\cdot\text{g}^{-1}$	4.946	5.676	4.844
Total Intrusion Volume, $\text{mL}\cdot\text{g}^{-1}$	0.155	0.158	0.112
Median Pore Diameter (Volume), μm	0.838	0.485	0.144
Median Pore Diameter (Area), μm	0.018	0.028	0.065
Average Pore Diameter ($4V/A$), μm	0.125	0.111	0.093
Bulk Density at 1.53psia, $\text{g}\cdot\text{mL}^{-1}$	1.71	1.17	2.09
Apparent (skeletal) Density, $\text{g}\cdot\text{mL}^{-1}$	2.33	1.44	2.74
Porosity, %	26.5	18.5	23.5
Steam Volume Used, %	46	30	45

3.2.7 Thermogravimetric (TG) analysis

The thermal properties of GWC IPs embedded with 0.5% CuO and 1% ZnO NPs was determined by TG analysis and the thermal decomposition of the materials was calculated. The spectra were divided into four different regions (**Fig. 3.9a**). The first region up to 120 °C shows the weight loss of samples attributed to evaporation of physically adsorbed water; c.a. 1.1% of its initial mass. In the second region from 120 to 440 °C, weight loss of samples was c.a. 2.1% at a constant rate. However, water evaporation may still occur at higher temperatures due to the fact that remaining water is either bound tightly in pores or is less able to diffuse to the surface. The water weight loss is attributed to the de-hydroxylation of the chemically bound silicon-hydroxyl group giving (silicon-oxygen-silicon) bridge with loss of water [Assaedi et al., 2016; Sultana et al., 2016]. Limited gel formation is justified by the limited weight loss of hydrated sodium aluminosilicate gel confirming again relative low compressive strength of GWC IPs. GWC IPs embedded with NPs showed lower thermal stability compared to the control. Despite low macroporosity of GWC IPs embedded with NPs, mesoporosity is high thus their ability to retain strong physically bonded water is reduced. The curve of 0.5% CuO NPs GWC IPs shifted slightly to a higher temperature (**Fig. 3.9a**, zoomed area) than the control. This may be attributed to the effect of NPs filling the voids, producing relatively dense IP. In the third range (440 to 800 °C) removal of chemically bound water occurs [Abdullah et al., 2020], indicating that calcium carbonate decomposes to calcium oxide [Kirboga et al., 2013]. The weight loss of 1% ZnO NPs GWC IPs was higher (38%) (**Fig. 3.9a**) compared to GWC IPs (control) with 0.5% CuO (36.2%). The decrease in weight of ZnO

NPs GWC IPs was at a relatively high rate. These changes can be attributed to the absorption of water prevailing in the channels of the matrix by NPs due to high surface area of NPs [Zidi et al., 2020]. In the fourth region (800 to 900 °C) no further weight loss was observed. The curve of 1% ZnO NPs GWC IPs is steeper at lower temperature compared to the control, as presented in DTA graph (Fig. 3.9b). The mesoporosity of IPs matrix was increased by the addition of NPs and thus the ability to retain water is decreased. Such results are in agreement with BET analysis.

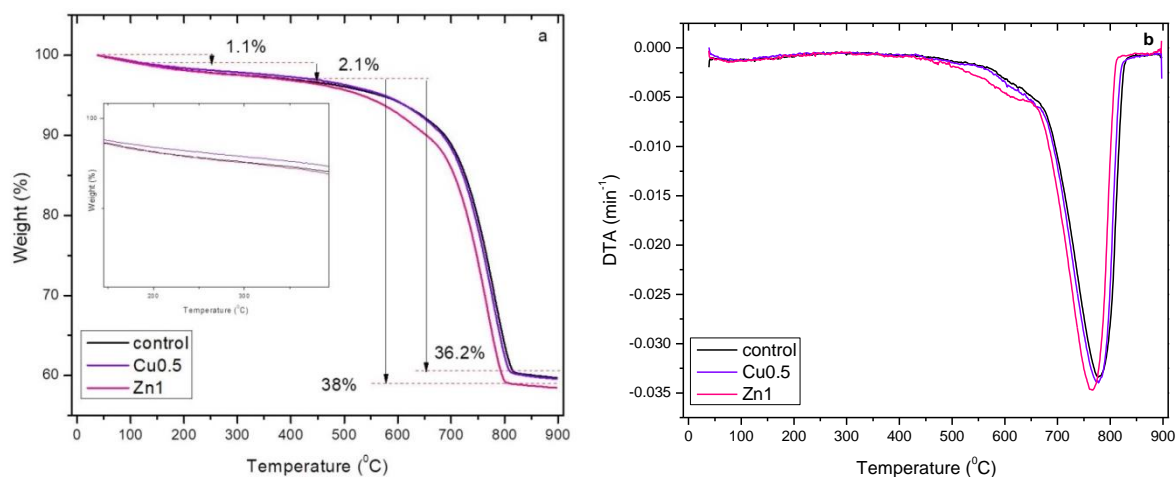


Figure 3.9: (a) Thermogravimetric (TG) analysis of GWC IP embedded with 0.5% CuO and 1% ZnO NPs; (b) DTA: derivative thermogravimetric analysis, the ratio of mass loss rate of sample to initial mass (min^{-1}) measured.

3.2.8 Antibacterial activity

The *E. coli* growth in the presence of GWC IPs embedded with CuO and ZnO NPs after 24 h incubation at 37 °C is presented (Fig. 3.10). 0.5% and 1% CuO NPs embedded in GWC IPs partially eliminated *E. coli* growth. However, high bacterial populations were observed in samples of ZnO NPs GWC IPs. These results may be attributed to the low amount of 1% and 2% ZnO NPs that were used under selected experimental conditions.

Uncoated beads (GWC IPs, control) also had significant inhibition capacity (98%) for *E. coli* growth in comparison to *E. coli* growth solely in the liquid culture. IPs possess alkali pH values when in contact with aqueous media, suggesting inhibition of bacterial growth [Poggetto et al., 2021]. Prior to antibacterial study, acid washing of NPs GWC IPs samples was carried out. Particularly, high alkalinity of fresh concrete/mortar and/or IPs at an early age limit bacterial growth. However, the pH of IPs and/or concrete/mortar IPs may be slowly reduced at long run by the effect of CO₂ and H₂S gas and thus, bacteria may evolve [Adak et al., 2015]. At alkaline pH death of *E. coli* bacteria is expected. Exposure of Gram-negative bacteria such as *E. coli* to high pH (i.e., 0.025 M NaOH) destroys cell membranes and causes leakage of the internal contents of cells [Sharma & Beuchat, 2004]. Additionally previous study showed that CuO nanorods preparation at 2M NaOH revealed significant antibacterial potential against *Salmonella typhimurium* and *Staphylococcus aureus* strains [Sonia et al., 2014]. ZnO NPs in metakaolin-based geopolymers may act as antibacterial agent limiting the growth of bacteria [Nur & Sari, 2017]. ZnO NPs coupled with a number of influenced factors such as particle size, concentration, morphology among others, confer significant toxicity to bacteria such as *E. coli* [Sirelkhatim et al., 2015].

Flower-shaped (CuO NPs in this study) to rod-like and spherical (in this study) ZnO nanostructures exhibit higher antibacterial activity against *E. coli* [Sirelkhatim et al., 2015]. In this study however, ZnO NPs did not exhibit antibacterial properties against *E. coli*. In agreement with a previous study

[Asamoah et al., 2020] ZnO NPs (of 21 nm in size) demonstrated no antibacterial activity against *E. coli*. Prior to *E. coli* growth experiments, Zn ions in the leachates were not detected. These results are in agreement with Hg porosimetry measurements, in which ZnO NPs GWC IPs had higher bulk and/or apparent density and thus a more compact structure in comparison to CuO NPs GWC IPs. However, Cu ions (1.1 and $1.8 \text{ mg}\cdot\text{L}^{-1}$) in the leachates were determined for GWC IPs embedded with 0.5% and 1% CuO NPs, respectively. Release of ionic Cu from copper-rich surfaces in the culture medium has also been suggested as a reason for their antimicrobial effect [Meghana et al., 2015]. Leaching of Cu ions from CuO NPs GWC IPs may explain the mechanism of CuO NPs antibacterial effect. Metal ion release in relation to oxidative stress induction and/or non-oxidative mechanisms may simultaneously occur explaining NPs antibacterial behavior [Javadhesari et al., 2019].

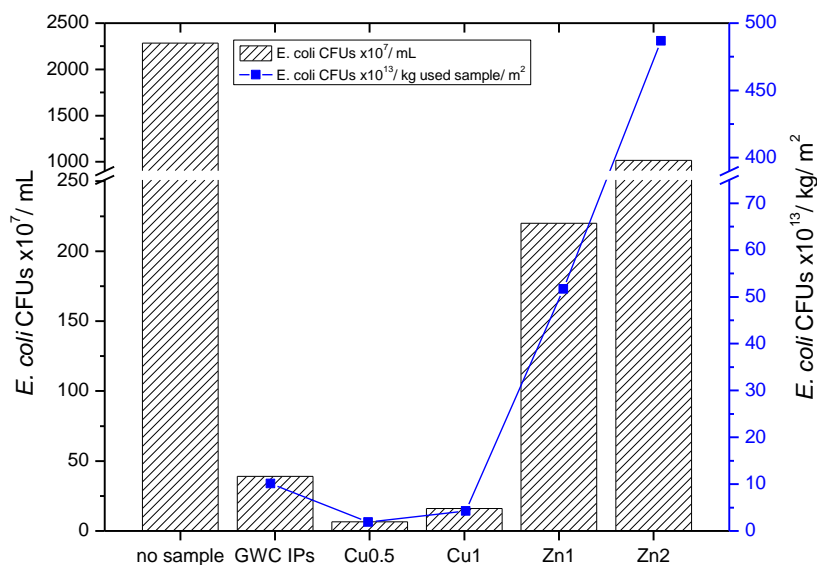


Figure 3.10: *E. coli* bacteria growth in the presence of GWC IPs embedded with CuO and ZnO NPs (*E. coli* CFUs/mL); (*E. coli* CFUs/kg used material/ m^2) as a function of NPs loading in GWC IPs (in disks).

Conclusions

The effect of CuO- and ZnO-nanoparticles on the mechanical and structural properties of alkali activated ground waste concrete waste was evaluated. GWC IPs in which 1% ZnO NPs were embedded showed a relative increase in compressive strength up to 23 MPa compared to GWC IPs with and without CuO NPs. The addition of CuO and/or ZnO NPs improved the interaction between NPs and inorganic polymer matrix, as indicated by shifts of the main peaks according to the obtained XRD patterns. Due to the poor content of aluminosilicate components in the raw material, limited inorganic polymerization is expected as was confirmed by Raman analysis. However, broadening of the main band can suggest the formation of differently structured material associated with the addition of NPs into IPs matrix. GWC IPs doped with 0.5% CuO NPs and 1% ZnO NPs exhibited a relatively dense structure and morphology with low water absorption. The homogeneity of a dense microstructure of NPs GWC IPs was evident by SEM imaging. The addition of NPs into GWC IPs matrix resulted in the augmentation of the mesoporosity of matrix thus a relative increase of compressive strength of the matrix was expected. Total intrusion volume of 1% ZnO NPs GWC IPs was lower due to the better void filling effect of ZnO NPs compared to CuO NPs. Porosity measurements were in agreement with compressive strength measurements. The incorporation of CuO and ZnO NPs suggested thermal stability and relatively improved thermal properties of IPs. GWC IPs embedded with 0.5% and 1% CuO NPs had positive antimicrobial properties that produced bacteria reduction as high as 80%.

Towards circular economy, IPs binders are considered eco-friendly, non-hazardous, cost effective, and durable building materials that may have wide applications in repair and/or restoration cases in construction building and road materials and pavements. Development of IPs from carbonate materials have been less explored. Some benefits of using carbonate-rich wastes such as ground waste concrete in IPs consist of improving structural quality and load bearing and reducing maintenance cost and extending life. Beyond the added benefit of waste management, the proposed IPs technology is an effective method for converting wastes into useful products. Additionally, IPs in which NPs are embedded may also be applied in functional surface applications such as floors and walls in houses and hospital facilities and/or marine concrete structures with antibacterial efficiency.

References

- Abdullah et al., 2020. XRD and TG-DTA study of new alkali activated materials based on fly ash with sand and glass powder. *Materials* 2020, 13, 343, doi:10.3390/ma13020343.
- Adak et al., 2015. Anti-microbial efficiency of nano silver–silica modified geopolymer mortar for eco-friendly green construction technology. *RSC Adv.* 5, 64037–64045, doi:10.1039/c5ra12776a.
- Ahmari et al., 2012. Production of geopolymeric binder from blended waste concrete powder and fly ash. *Constr Build. Mater* 35, 718–729.
- Aïtcin, 2000. Cements of yesterday and today. *Concrete of tomorrow. Cement Concrete Res.* 30, 1349–1359.
- Amran et al., 2020. Clean production and properties of geopolymer concrete; A review. *J. Clean. Prod.* 251, 119679, doi:10.1016/j.jclepro.2019.119679.
- Andrew, 2018. Global CO2 emissions from cement production. *Earth Syst. Sci. Data* 10, 195–217, doi:10.5194/essd-10-195-2018.
- Aredes et al., 2015. Effect of cure temperature on the formation of metakaolinite-based geopolymer. *Ceram. Int.* 2015, 41, 7302–7311, doi:10.1016/j.ceramint.2015.02.022.
- Ariffin et al., 2013. Sulfuric acid resistance of blended ash geopolymer concrete. *Constr. Build. Mater.* 43, 80–86.
- Armayani & Pratama, 2017. The properties of nano silver (Ag)-geopolymer as antibacterial composite for functional surface materials. *MATEC Web Conf.* 97, 1010, doi:10.1051/mateconf/20179701010.
- Arnoult et al., 2018. How to control the geopolymer setting time with the alkaline silicate solution. *J. Non-Crystalline Solids* 2018, 495, 59–66, doi:10.1016/j.jnoncrysol.2018.02.036.
- Asamoah et al., 2020. Synthesis and characterization of zinc and copper oxide nanoparticles and their antibacteria activity. *Results Mater.* 7, 100099, doi:10.1016/j.rinma.2020.100099.
- Assaedi & Shaikh, 2016. Low, I. Effect of nano-clay on mechanical and thermal properties of geopolymer. *J. Asian Ceram. Soc.* 4, 19–28, doi:10.1016/j.jascers.2015.10.004.
- Bakharev, 2005. Durability of geopolymer materials in sodium and magnesium sulfate solutions. *Cem. Concr. Res.* 35, 1233–1246.
- Behera et al., 2014. Recycled aggregate from C&D waste & its use in concrete – A breakthrough towards sustainability in construction sector: A review. *Constr. Build. Mater.* 68, 501–516.
- Carbone et al., 2017. Antimicrobial power of Cu/Zn mixed oxide nanoparticles to *Escherichia coli*. *Environ. Nanotechnol. Monit. Manag.* 7, 97–102, doi:10.1016/j.enmm.2017.01.005.
- Cerna et al., 2019. Development of nanosilver-coated geopolymer beads (AgGP) from fly ash and baluko shells for antimicrobial applications. *MATEC Web Conf.* 268, 05003, doi:10.1051/mateconf/201926805003.
- Chang et al., 2012. The toxic effects and mechanisms of CuO and ZnO nanoparticles. *Materials*, 5, 2850–2871, doi:10.3390/ma5122850.
- Couto & Couto, 2010. Guidelines to Improve Construction and Demolition Waste Management in Portugal, Process Management, Maria Pomffyova, IntechOpen, doi: 10.5772/8456. Available from: <https://www.intechopen.com/chapters/9673>.
- Cristelo et al., 2018. Stabilisation of construction and demolition waste with a high fines content using alkali activated fly ash. *Constr Build Mater* 170, 26–39.
- Cullity & Stock, 2002. *The Elements of X-ray Diffraction*, 3rd ed.; Wesley, Pearson New International Press: Edinburgh, UK, 2002.

- Davidovits, 1991. Geopolymers: Inorganic polymeric new materials. *J. Thermal Anal. Calorim* 37, 1633–1656.
- Davidovits, 2015. False Values on CO₂ Emission for Geopolymer Cement/Concrete; Technical Paper; Geopolymer Institute Library: Saint-Quentin, France, 29 June 2015; pp. 1–9.
- Davidovits, 2017. Geopolymers: Ceramic-like inorganic polymers. *J. Ceram. Sci. Technol.* 8, 335–350.
- Davidovits, 2018. Why Alkali-Activated Materials (AAM) are not geopolymers. Technical Paper #25, Geopolymer Institute Library, www.geopolymer.org; DOI: 10.13140/RG.2.2.34337.25441.
- Deb et al., 2016. Sorptivity and acid resistance of ambient-cured geopolymer mortars containing nano-silica. *Cem. Concr. Compos.* 2016, 72, 235–245, doi:10.1016/j.cemconcomp.2016.06.017.
- Dörner et al., 2019. Cost-effective sol-gel synthesis of porous CuO nanoparticle aggregates with tunable specific surface area. *Sci. Rep.* 2019, 9, 1–13, doi:10.1038/s41598-019-48020-8.
- Du et al., 2019. Nanotechnology in cement-based materials: A review of durability, modeling, and advanced characterization. *Nanomaterials* 9, 1213, doi:10.3390/nano9091213.
- EU-28, 2016. Waste generation by economic activities and households. [https://ec.europa.eu/eurostat/statistics-explained/index.php?title=File:Waste_generation_by_economic_activities_and_households,_EU-28,_2016_\(%25\).png&direction=next&oldid=413561](https://ec.europa.eu/eurostat/statistics-explained/index.php?title=File:Waste_generation_by_economic_activities_and_households,_EU-28,_2016_(%25).png&direction=next&oldid=413561) (accessed on 30 December 2021)
- EU, 2020. A New Circular Economy Action Plan for a Cleaner and More Competitive Europe; European Commission: Brussels, Belgium.
- Eurostat, 2019a. Generation of Waste by Waste Category, Hazardousness and NACE Rev. 2 Activity [env_wasgen]. Available online: https://appsso.eurostat.ec.europa.eu/nui/show.do?dataset=env_wasgen&lang=en (accessed on 4 August 2021)
- Farhana et al., 2019. Improvement in the performance of solar collectors with nanofluids—A state-of-the-art review. *Nano Struct. Nano-Objects* 18, 100276, doi:10.1016/j.nanoso.2019.100276.
- Galiano et al., 2016. Contributions to the study of porosity in fly ash-based geopolymers. Relationship between degree of reaction, porosity and compressive strength. *Materiales Construcción* 66, 098, doi:10.3989/mc.2016.10215.
- Ganiron, 2015. Recycling concrete debris from construction and demolition waste. *Int. J. Adv. Sci. Technol.* 77, 7–24.
- Geetha et al., 2016. Green mediated synthesis and characterization of ZnO nanoparticles using euphorbia jatropa latex as reducing agent. *J. Sci. Adv. Mater. Devices* 2016, 1, 301–310, doi:10.1016/j.jsamd.2016.06.015.
- Gunasekara et al., 2019. Effect of curing conditions on microstructure and pore-structure of brown coal fly ash geopolymers. *Appl. Sci.* 2019, 9, 3138, doi:10.3390/app9153138.
- Gutiérrez et al., 2020. Evaluation of the antibacterial activity of a geopolymer mortar based on metakaolin supplemented with TiO₂ and CuO particles using glass waste as fine aggregate. *Coatings* 10, 157, doi:10.3390/coatings10020157.
- Guzmán-Aponte et al., 2017. Metakaolin-based geopolymer with added TiO₂ particles: Physicomechanical characteristics. *Coatings* 7, 233, doi:10.3390/coatings7120233.
- Jabbar, 2016. Synthesis of CuO nano structure via sol-gel and precipitation chemical methods. *Al-Khwarizmi Eng. J.* 12, 126–131.
- Janáky & Rajeshwar, 2015. The role of (photo)electrochemistry in the rational design of hybrid conducting polymer/semiconductor assemblies: From fundamental concepts to practical applications. *Prog. Polym. Sci.* 43, 96–135, doi:10.1016/j.progpolymsci.2014.10.003.

- Javadhesari et al., 2019. Antibacterial activity of ultra-small copper oxide (II) nanoparticles synthesized by mechanochemical processing against *S. aureus* and *E. coli*. *Mater. Sci. Eng. C* 2019, 105, 110011, doi:10.1016/j.msec.2019.110011.
- Jindal & Sharma, 2020. The effect of nanomaterials on properties of geopolymers derived from industrial by-products: A state-of-the-art review. *Constr. Build. Mater.* 252, 119028, doi:10.1016/j.conbuildmat.2020.119028.
- Khan et al., 2019. Nanoparticles: Properties, applications and Toxicities. *Arab. J. Chem.* 12, 908–931.
- Kirboga et al., 2013. Investigation of calcium carbonate precipitation in the presence of carboxymethyl inulin. *Cryst. Eng. Comm.* 15, 3678–3686, doi:10.1039/c3ce27022j.
- Komnitsas et al., 2007. Geopolymerisation of low calcium ferronickel slags. *J. Mater. Sci.* 42, 3073–3082.
- Komnitsas & Zaharaki, 2007. Geopolymerisation. A review and prospects for the minerals industry. *Miner. Eng.* 20, 1261–1277.
- Komnitsas, 2011. Potential of geopolymer technology towards green buildings and sustainable cities. *Procedia Eng.* 21, 1023–1032.
- Komnitsas et al., 2013. Effect of sulphate and nitrate anions on heavy metal immobilisation in ferronickel slag geopolymers. *Appl. Clay Sci.* 73, 103–109.
- Komnitsas et al., 2015. Effect of synthesis parameters on the quality of construction and demolition wastes (CDW) geopolymers. *Adv. Powder Technol.* 26, 368–376, doi:10.1016/j.apt.2014.11.012.
- Komnitsas, 2016. Co-valorization of marine sediments and construction & demolition wastes through alkali activation. *J. Environ. Chem. Eng.* 4, 4661–4669.
- Komnitsas et al., 2019. Assessment of alkali activation potential of a Polish ferronickel slag. *Sustainability* 2019, 11, 1863, doi:10.3390/su11071863.
- Komnitsas et al., 2020. Factors affecting co-valorization of fayalitic and ferronickel slags for the production of alkali activated materials. *Sci. Total Environ.* 721, 137753.
- Konsta-Gdoutos, 2014. Nanomaterials in self-consolidating concrete: A state-of-the-art review. *J. Sustain. Cem. Mater.* 3, 167–180, doi:10.1080/21650373.2014.909751.
- Kosor et al., 2016. Geopolymerization index of fly ash geopolymers. *Vib. Spectrosc.* 2016, 85, 104–111, doi:10.1016/j.vibspec.2016.04.005.
- Liu et al., 2020. Review on the research progress of cement-based and geopolymer materials modified by graphene and graphene oxide. *Nanotechnol. Rev.* 9, 155–169, doi:10.1515/ntrev-2020-0014.
- Lowell & Shields, 1991. Interpretation of mercury porosimetry data. *Powder Surf. Area Porosity* 2, 99–120, doi:10.1007/978-94-015-7955-1_11.
- Ma et al., 2018. Structural and material performance of geopolymer concrete: A review. *Constr Build. Mater.* 186, 90–102.
- Maddalena et al., 2018. Can Portland cement be replaced by low-carbon alternative materials? A study on the thermal properties and carbon emissions of innovative cements. *J. Clean. Prod.* 186, 933–942, doi:10.1016/j.jclepro.2018.02.138.
- Mavridou, et al., 2015. Construction and demolition (C&D) waste: Potential uses and current situation in Greece and Cyprus. In *Proceedings of the International Conference Industrial Waste & Wastewater Treatment & Valorisation*, Crete Island, Greece, 21–23 May 2015.
- Meghana et al., 2015. Understanding the pathway of antibacterial activity of copper oxide nanoparticles. *RSC Adv.* 5, 12293–12299, doi:10.1039/c4ra12163e.
- Mehta & Siddique, 2016. An overview of geopolymers derived from industrial by-products. *Constr. Build. Mater.* 127, 183–198.

- Mendes et al., 2015. Nanoparticles in cement based materials: A review. *Rev. Adv. Mater. Sci.* 40, 89–96.
- Mohajerani et al., 2019. Recycling waste materials in geopolymer concrete. *Clean Technol. Environ. Policy* 21, 493–515.
- Nawaz et al., 2020. Geopolymers in construction—recent developments. *Constr. Build. Mater.*, 260, 120472, doi:10.1016/j.conbuildmat.2020.120472.
- Ng et al., 2018. A review on microstructural study and compressive strength of geopolymer mortar, paste and concrete. *Constr. Build. Mater.* 186, 550–576.
- Niveditha & Koniki, 2020. Effect of Durability properties on geopolymer concrete—a review. *E3S Web Conf.* 2020, 184, 01092, doi:10.1051/e3sconf/202018401092.
- Noeiaghahi et al., 2017. Biogenic deterioration of concrete and its mitigation technologies. *Constr. Build. Mater.* 149, 575–586, doi:10.1016/j.conbuildmat.2017.05.144.
- North & Swaddle, 2000. Kinetics of silicate exchange in alkaline aluminosilicate solution. *Inorg. Chem.* 39, 2661–2665.
- Nur & Sari, 2017. Development of geopolymers composite based on metakaolin-nano ZnO for antibacterial application. *IOP Conf. Series Mater. Sci. Eng.* 180, 12289, doi:10.1088/1757-899x/180/1/012289.
- Pacheco-Torgal et al., 2012. Are geopolymers more suitable than Portland cement to produce high volume recycled aggregates HPC? *Constr. Build. Mater.* 36, 1048–1052.
- Phair, 2006. Green chemistry for sustainable cement production and use. *Green Chem.* 8, 763–780
- Poggetto et al., 2021. Efficient addition of waste glass in MK-based geopolymers: Microstructure, antibacterial and cytotoxicity investigation. *Polymers* 13, 1493, doi:10.3390/polym13091493.
- Qadry & Kharisma, 2019. The properties of geopolymer-cuo nanoparticles as a functional composite. *Mater. Sci. Forum* 967, 281–285, doi:10.4028/www.scientific.net/msf.967.281.
- Ramezani-pour & Moeini, 2018. Mechanical and durability properties of alkali activated slag coating mortars containing nanosilica and silica fume. *Constr. Build. Mater.* 163, 611–621.
- Rashad, 2013. Effects of ZnO₂, ZrO₂, Cu₂O₃, CuO, CaCO₃, SF, FA, cement and geothermal silica waste nanoparticles on properties of cementitious materials—A short guide for Civil Engineer. *Constr. Build. Mater.* 48, 1120–1133.
- Rashad, 2019. Effect of nanoparticles on the properties of geopolymer materials. *Mag. Concr. Res.* 71, 1283–1301, doi:10.1680/jmacr.18.00289.
- Scrivener et al., 2018. Eco-efficient cements: Potential economically viable solutions for a low-CO₂ cement-based materials industry. *Cem. Concr. Res.* 114, 2–26, doi:10.1016/j.cemconres.2018.03.015.
- Shafeek et al., 2020. Influence of ZnO nanoparticle ratio and size on mechanical properties and whiteness of White Portland Cement. *Appl. Nanosci.* 10, 3603–3615, doi:10.1007/s13204-020-01444-5.
- Sharma & Beuchat, 2004. Sensitivity of Escherichia coli O157:H7 to commercially available alkaline cleaners and subsequent resistance to heat and sanitizers. *Appl. Environ. Microbiol.* 70, 1795–1803, doi:10.1128/aem.70.3.1795-1803.2004.
- Shehata et al., 2021. Recent progress in environmentally friendly geopolymers: A review. *Sci. Total Environ.* 762, 143166, doi:10.1016/j.scitotenv.2020.143166.
- Sikora et al., 2018. Antimicrobial activity of Al₂O₃, CuO, Fe₃O₄, and ZnO nanoparticles in scope of their further application in cement-based building materials. *Nanomaterials* 8, 212, doi:10.3390/nano8040212.

- Singh et al., 2015. Geopolymer concrete: A review of some recent developments. *Constr. Build. Mater.* 85, 78–90, doi:10.1016/j.conbuildmat.2015.03.036.
- Singh et al., 2018a. Effect of nanomaterials on the properties of geopolymer mortars and concrete. *Mater. Today Proc.* 2018, 5, 9035–9040, doi:10.1016/j.matpr.2017.10.018.
- Singh et al., 2018b. ‘Green’ synthesis of metals and their oxide nanoparticles: Applications for environmental remediation. *J. Nanobiotechnol.* 16, 84, doi:10.1186/s12951-018-0408-4.
- Sirelkhatim et al., 2015. Review on zinc oxide nanoparticles: Antibacterial activity and toxicity mechanism. *Nano-Micro Lett.* 7, 219–242, doi:10.1007/s40820-015-0040-x.
- Sonia et al., 2014. Effect of NaOH concentration on structural, surface and antibacterial activity of CuO nanorods synthesized by direct sonochemical method. *Superlattices Microstruct.* 66, 1–9, doi:10.1016/j.spmi.2013.10.020.
- Sotelo-Piña et al., 2018. Geopolymers: Past, present, and future of low carbon footprint eco-materials. In *Handbook of Ecomaterials*; Springer: Berlin/Heidelberg, Germany, pp. 1–21.
- Soultana et al., 2019. Properties of inorganic polymers produced from brick waste and metallurgical slag. *Minerals* 9, 551, doi:10.3390/min9090551.
- Sun et al., 2014. A Raman spectroscopic comparison of calcite and dolomite. *Spectrochim. Acta Part A Mol. Biomol. Spectrosc.* 117, 158–162, doi:10.1016/j.saa.2013.08.014.
- Tam et al., 2018. A review of recycled aggregate in concrete applications (2000–2017). *Constr. Build. Mater.* 2018, 172, 272–292.
- Tan et al., 2020. Current development of geopolymer as alternative adsorbent for heavy metal removal. *Environ. Technol. Innov.* 18, 100684, doi:10.1016/j.eti.2020.100684.
- Vavouraki, 2020. Utilization of industrial waste slags to enhance ground waste concrete-based inorganic polymers. *J. Sustain. Met.* 6, 383–399, doi:10.1007/s40831-020-00281-8.
- Wong et al., 2018. Potential use of brick waste as alternate concrete-making materials: A review. *J. Clean. Prod.* 195, 226–239.
- Wu et al., 2019. Geopolymer, green alkali activated cementitious material: Synthesis, applications and challenges. *Constr. Build. Mater.* 224, 930–949, doi:10.1016/j.conbuildmat.2019.07.112.
- Xie & Fang, 2019. Nanomaterials applied in modifications of geopolymer composites: A Review. *Aust. J. Civ. Eng.* 17, 32–49, doi:10.1080/14488353.2019.1614353.
- Zaharaki et al., 2016. Valorization of construction and demolition (C&D) and industrial wastes through alkali activation. *Constr. Build. Mater.* 121, 686–693, doi:10.1016/j.conbuildmat.2016.06.051.
- Zailan et al., 2019. Influence of ZnO nanoparticles on mechanical properties and photocatalytic activity of self-cleaning ZnO-based geopolymer paste. *J. Inorg. Organomet. Polym. Mater.* 30, 2007–2016, doi:10.1007/s10904-019-01399-3.
- Zhuang et al., 2016. Fly ash-based geopolymer: clean production, properties and applications. *J. Clean. Prod.* 125, 253–267.
- Zidi et al., 2019. Synthesis of nano-alumina and their effect on structure, mechanical and thermal properties of geopolymer. *J. Asian Ceram. Soc.* 7, 524–535, doi:10.1080/21870764.2019.1676498.
- Zidi et al., 2020. Effect of nano-ZnO on mechanical and thermal properties of geopolymer. *J. Asian Ceram. Soc.* 8, 1–9, doi:10.1080/21870764.2019.1693682.